POLITECNICO DI TORINO

Dipartimento di Elettronica e Telecomunicazioni

Master degree course in Nanotechnologies for ICTs

Master Degree Thesis

Multiphase colloidal system: electrical charaterization of triboelectric and ferromagnetic colloids

CERES Project

Supervisor
Prof. Carlo RICCIARDI

Candidate
Luca CECCHINI

Supervisor
Istituto Italiano di Tecnologia
Center for Sustainable Future Tecnologies
Prof. Alessandro CHIOLERIO

ANNO ACCADEMICO 2018 − 2019

Will is the magic that transforms energy into becoming.

Abstract

The present Master Thesis work is a dissertation on the electrical characterization of a multi-phase colloidal system for energy harvesting, based on thermomagnetic and triboelectric effects.
The research program (**C**olloidal **E**ne**R**g**E**tic **S**ystem - CERES Project) has been conducted within the Center for Sustainable Future Technologies (CSFT) at Istituto Italiano di Tecnologia (IIT) of Turin.

This work is divided in three main topics: the first one is a complete description of the physical background involved in the thermomagnetic and triboelectric energy harvesting; then, an elucidation on the colloidal systems has been proposed, focusing on the stability conditions and the related size effect; finally, it is presented an experimental setup for the electrical characterization of the output power of the recovery system and the correlated results.

Moreover, a new representation of the governing equation involved in the thermomagnetic motion generation and in the electromotive force extraction is shown.

The idea behind the CERES system is to exploit the physical properties of colloids in order to recover energy from low enthalpy heat sources. In particular, it is possible to locate this project within the Waste Heat to Power framework. This can be possible considering the thermomagnetic properties of ferrofluids, a suspension of magnetic nanoparticles dispersed in a liquid solvent and the triboelectric properties of TiO_2 nanopowder dispersed in pure water.
Since the magnetization of the particles is temperature dependent, the interaction between a magnetic field and thermal gradients produces cycling magnetic forces. In this way, the variation of the particles momentum can be directly converted into electric energy. However, the thermally activated fluid motion and the recovery mechanisms are not linearly independent, because they both exploit the magnetic field for the flow generation (thermomagnetic effects) and for the energy harvesting (Faraday-Neumann-Lenz law). To have a better knowledge about the feasibility and energetic sustainability of this waste heat recovery, it is also important to define the electrical behaviour of the output power of the system.

The experimental phase dealt with the setup of a Fluorinated Ethylene Propylene (FEP) pipe, in which flow is induced by means of a controlled peristaltic pump. A network of magnets was placed in the extraction region, where a solenoid is installed around the pipe. To measure also the capacitive component of the system, an aluminum ring was anchored on the pipe and used as electrode (Single-Electrode Mode).

From the electrical characterization it follows that the magnetic inductance permits to reach an output power per unit volume of 14.64 μW/L and from the triboelectric effect it is possible extract an output power per unit surface of 1.212 μW/m^2.

To conclude, this kind of characterization can open new lines of research in the CERES Project, including different choice of the materials that can be associated to the tank wall and the related functionalization of the active surface with nanostructures, the synthesis of a stable colloidal solution that includes magnetic and tribeoelectric properties, a validation of the results using a multiphysics CFD simulation and the installation of the recovery mechanisms on the real prototype.

Contents

List of Tables

List of Figures

9

Chapter 1

Introduction

1.1   A matter of Energy

Energy is an integral part of our everyday life, being one of the most fundamental needs, including our physiological activity. In the last 20 years, energy related issues, including demand and accessibility, consumption and consciousness of use, have become a topic of paramount importance. Most of the governments grant increasingly wide budgets to carry out evaluations about the so-called Energy Problem and the related Global Warming. Energy is the driving force of the development of global economies and the world energy crisis has brought enormous economic losses globally due to over-exploitation and over-use of energy.

To highlight the critical aspect of energy issues, we may recall that the world energy consumption in 2040 is expected to surpass 200,000 TWh/year where the industry sector (expected to increase by an 18 % from 2015 to 2040) would play for more than 50 % of that amount [1]. In order to support long-term energy efficiency improvement and reduction of energy consumption, action plans must be established. The key point for global energy demand can be guaranteed through long period planning and huge investments to make it reliable, available and affordable. Furthermore, due to global warming, increasing energy costs and green politics, the continuous research for more sustainable and cleaner energy sources is an ever-growing worldwide interest.

According with Bostjan et al.[2], most of the energy production is nowadays derived from fossil fuels, while renewable sources represent less than a quarter of global consumption. So, since the energy requirement for manufacturing and living has never been cut, it is necessary to improve the efficiency of the processes rather than reduce energy for production. Moreover, this apparent unstoppable increasing trend of energy demand has a direct impact on the environmental conditions and on the living conditions of people.

The creation of a common approach with a new attitude towards our fragile natural environment is demanded. Alongside with the increasing consumption of primary

energy, the amount of waste heat increases, representing therefore a greater economic and ecologic potential for utilization.
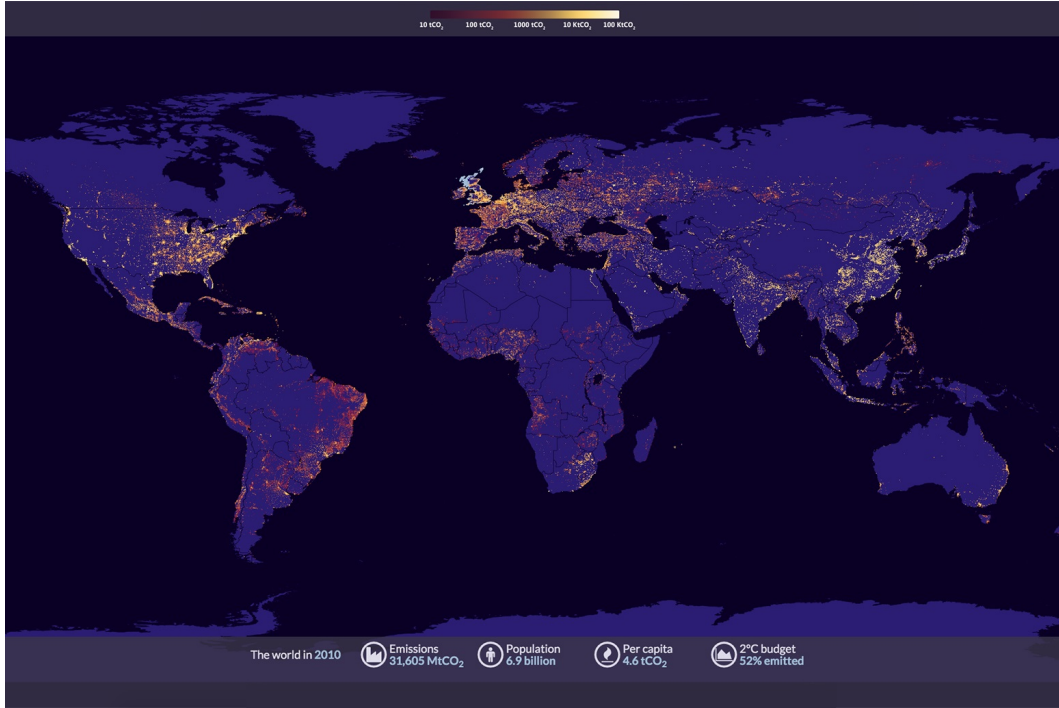
Figure 1.1. Map of Global Energy Consumption (2010). The emission data come from the Carbon Dioxide Information Analysis Center (CDIAC) and they are evaluated mainly from fuel-fossil burning.

From a thermodynamic point of view, waste heat is defined as low-grade exergetic source, so the maximum useful work that is possible to extract from this source is negligible and it is lost in the environment. So, before is exploited, waste heat should be avoided through an energetic optimization of processes. This can be done in different ways, as for example processes with needs-based controls, design and process operation. However, waste heat represent a significant potential in the renewable sources field.

From an environmental point of view, the enormous amount of waste heat injected in the environment has also the side effect of locally increasing the atmosphere temperature. In fact, the solubility of carbon dioxide in water decreases as temperature increases and the amount of gas in equilibrium at standard pressure conditions is therefore directly affected by waste heat, amplifying the effects of global warming. The most important greenhouse gas, in reason of its specific heat capacity and volume content in the atmosphere, is water vapour. At 298 K and 50 % relative humidity, we have one molecule of CO_2 every 2,143 molecules of water vapour,

13

whose greenhouse effect is more than double (2.19 times) that of carbon dioxide. To have an idea of the abundance of this source, between 60 to 30 % of the overall energy consumed is wasted into the environment as heat.

Considering an analysis based on conservative parameters, it is possible to estimate that a possible amount of waste heat can be recovered and transformed in electric energy for a value of around 20 TWh/year, generating more than 2.64 billion EUR if this electricity is sold to industries (@ 0.125 EUR/kWh which is the 2015 cost towards industrial consumption) or more than 4.4 billion EUR if sold to households (@ 0.221 EUR/kWh which is the 2015 cost towards households consumption).[3, 4, 5] The cost per kWh generated can be further increased considering an intelligent politics aimed to sustain research and development of integrated processed and investiment in equipment manifacturing.

1.2   CERES Project

The CERES Project (**C**olloidal **E**ne**R**g**E**tic **S**ystem) is defined within the so-called Low-Grade Waste Heat Recovery (WHR) frame, in which the thermal source is characterized by low enthalpy values. The general classification of WHR is based on the values of temperature of the heating source. In particular, considering that the low temperature of the thermodynamic system is defined as $T_L = 25$ °C, we can state that:

- Low grade: $T_H \leq 250$ °C
- Medium grade: 250 °C $< T_H \leq 650$ °C
- High grade: $T_H > 650$ °C

The idea behind this project is directly linked to the CAS concept (**C**olloidal **A**utonomous **S**ystem) [6], in which colloidal devices, properly protected from the external harsh environment by a deformable skin, are used in order to realize a revolutionary system for the purpose of liquid-robotics. With respect to the well known heavy-robotics, this kind of technology can be used in harsh environment applications, as space exploration, or the deepest zones of remotes lakes and oceans, or post-disaster rescue searches, or even in surgery operations [1]. From an energetic point of view, this autonomous system needs to be coupled with an energy harvesting/storage in an efficient way. So, the CERES idea came up from this point, where a multiphase colloidal system can recover energy from waste heat sources, using different recovery mechanisms, as the triboelectric effect and the magnetic induction.

In order to understand better how the CERES system works, it is interesting to do

---

[1]If the reader is interested in a more detailed analysis about CAS systems can consult the document [6].

a preliminary analysis on this project.

First of all, it is necessary to prototype a closed-system, which is able to exchange only electromagnetic and thermal energy with the outer environment, so it should be enclosed in a thin shell (acting as a skin). This concept is very similar to the prototyping of a magnetic confinement fusion reactor.
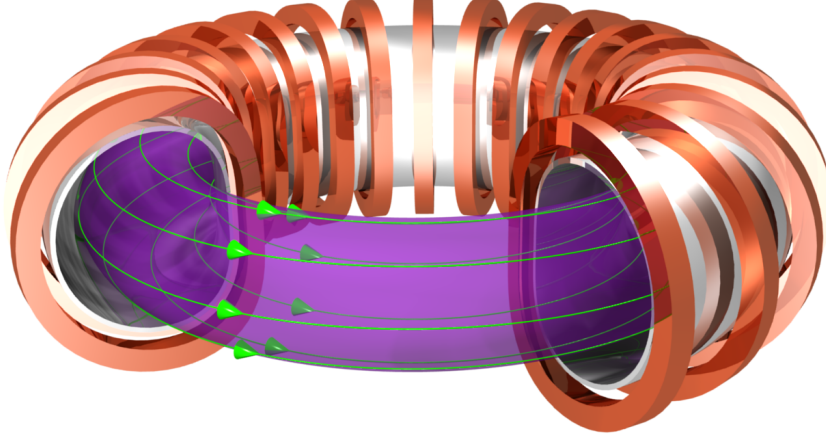
Figure 1.2. Example of the DOUGHNUT structure, inspired by the Tokamak structure.

The system is called DOUGHNUT (a**D**atptive c**O**lloidal acc**U**mulatin**G**/**H**arvesti**N**g **U**niT) and it can be defined as a Thermomagnetic Hydrodynamic Machine (THM), where a thermal source is able to set in motion a liquid colloidal solution. The peculiar properties of colloids allow to modify the physical behaviour of a carrier liquid, simply dispersing nanoparticles in a stable way inside this solution. The most suitable material for this application is the ferrofluid, that is a suspension of magnetic nanoparticles dispersed in non-magnetic solvents, which presents high magnetic susceptibility and maintains a paramagnetic behaviour under a specific temperature range.

By exchanging heat from a hot to a cold reservoir, it is possible to generate a temperature gradient inside this structure. Furthermore, applying an external magnetic field the system is perturbed statically, since the the fluid presents a magnetic behaviour.

So, the thermally generated motion can be associated mainly to a convection mechanism, where the buoyancy forces (thermal expansion of the fluid and gravitation) and the magnetic forces (magnetic field and thermomagnetic effect) allow to generate a thermomagnetic advection motion. The energy generated by this variation of momentum in the fluid can be extracted considering the time-variation of the magnetic flux (Faraday-Neumann-Lenz' law).

Chapter 2

Physical Background

2.1 Thermodynamics

2.1.1 General definitions

For the purposes of this thesis, we are interested in the collective behaviour of a closed system, in which it is possible to define and measure the evolution of different states according to the influence of external perturbations.

In all the systems there is a tendency to evolve towards states in which the properties are determined by intrinsic factors (equilibrium states). From a macroscopic point of view, it is possible to fully describe a time independent system by internal energy U, the volume V, the mole number $N_1, N_2, ..., N_r$ of the chemical components, the magnetic induction **B** and the electric displacement **D**.

The natural evolution of the states can be controlled and measured only if we assume the presence of boundaries and constraints, that in our case are defined by adiabatic walls and isothermal walls. The adiabatic walls guarantee the essential prerequisite for the measurability, i.e. no transfer of heat or mass of substances between a thermodynamic system and its surroundings. Instead, the isothermal walls define the temperature value in specific points and so it is possible to control the thermodynamic properties of the system. So, considering a closed system (constant mole numbers), it is possible to define the heat flux as the difference of the internal energy between two equilibrium states, diminished by the work done in that process. This is the well know **First law of Thermodynamics** [7]:

$$\delta Q = dU - \delta W. \tag{2.1}$$

This results in the fact that heat, like work are just a form of energy transfer. Therefore, once the energy is transferred to a system, it becomes indistinguishable between different sources. It is important to stress the fact that this formulation is valid only for quasi-static processes, so the system evolves slowly and quiescently

to a thermodynamic equilibrium. This implies also that in each instant of time, the system is in an equilibrium state.

The work that can be done to a system can be associated to different physical phenomena, depending on the properties of the material that we take into account. In particular, we can assume to have quasi-static mechanical work W_M, quasi-static magnetic work W_B, quasi-static electric work W_D and quasi-static chemical work W_c.

$$\delta W = \delta W_M + \delta W_B + \delta W_D + \delta W_c$$

$$\delta W = -pdV - \mathbf{m} \cdot d\mathbf{B} - \mathbf{p} \cdot d\mathbf{D} + \sum_{j=1}^{N} \mu_j dN_j \tag{2.2}$$

where p is the pressure (defined as negative), $\mathbf{m}$ is the magnetic dipole moment, $\mathbf{p}$ is the electric dipole moment and μ_j is the electrochemical potential of the j-th component.

Considering also the **Second law of Thermodynamics** [7], and so the Clausius' inequality, it is possible to define the quasi-static heat flux as function of the temperature T and the entropy S of the system. So, if we consider a reversible thermodynamic process, we obtain:

$$dS \geq \frac{dQ}{T} \qquad \underbrace{dQ = TdS}_{\text{Reversible}} \tag{2.3}$$

Therefore, combining the equations above, we obtain a differential formulation for the internal energy of a system:

$$dU = TdS - pdV - \mathbf{m} \cdot d\mathbf{B} - \mathbf{p} \cdot d\mathbf{D} + \sum_{j=1}^{N} \mu_j dN_j \tag{2.4}$$

We can observe that Eq.2.4 represent the total differential of the internal energy with respect to the so called **extensive parameters** X_i [7], that are parameters that depend on the system size and/or the amount of material inside the system. The Eq.2.4 is usually called fundamental equation.

$$U = U(S, V, \mathbf{B}, \mathbf{D}, N_1, N_2, \cdots, N_r) = U(S, X_1, \cdots, X_k) \tag{2.5}$$

On the other hand, the **intensive parameters** [7] are physical quantities that describe how the internal energy changes according to the extensive parameters. Hence, assuming that U is a differentiable function, it is possible to define:

$$\left(\frac{\partial U}{\partial S}\right) \equiv T \; ; \; -\left(\frac{\partial U}{\partial V}\right) \equiv p \; ; \; -\left(\frac{\partial U}{\partial B}\right) \equiv m \; ; \; -\left(\frac{\partial U}{\partial D}\right) \equiv \mathrm{p} \; ; \; \left(\frac{\partial U}{\partial N_j}\right) \equiv \mu_j$$

2.1.2 Euler equation and Maxwell relations

If we consider the homogeneous first order property of the fundamental equation:

$$U(\lambda S, \lambda X_1, \cdots, \lambda X_k) = \lambda U(S, X_1, \cdots, X_k) \tag{2.6}$$

it is possible to differentiate with respect to λ, rewriting Eq.2.4 in the so called Euler form:

$$U = TS - pV - \mathbf{m} \cdot \mathbf{B} - \mathbf{p} \cdot \mathbf{D} + \sum_{j=1}^{N} \mu_j N_j \tag{2.7}$$

We have to keep in mind that in the energy representation the extensive parameters play a role of mathematical independent variables, whereas the intensive parameters are derived concepts. So, the question is if it is possible to recast the mathematical formalism in such a way that intensive parameters replace the extensive one as independent variables. That is possible under a linearization condition, using the Legendre transformations [7]. The functions obtained in this way are defined as thermodynamic potentials.

Thermodynamic potentials   The Helmholtz free energy is the Legendre transform of U that replaces the entropy by the temperature as independent variable:

$$F \equiv U[T] \qquad F(T, V, \mathbf{m}, \mathbf{p}, N_1, N_2, \cdots) \qquad -S = \left(\frac{\partial F}{\partial T}\right) \qquad F = U - TS$$

It represents the maximum work that a system can do at constant volume and temperature.
The enthalpy is the Lengandre transform of U that replaces the volume by the pressure as independent variable:

$$H \equiv U[V] \qquad H(S, p, \mathbf{m}, \mathbf{p}, N_1, N_2, \cdots) \qquad V = \left(\frac{\partial H}{\partial p}\right) \qquad H = U + pV$$

It represents the capacity of a system to do non-mechanical work and to release heat.
The Gibbs free energy is the Legendre transform of U that replaces the temperature and the volume by the pressure as independent variable:

$$G \equiv U[T, p] \qquad G(T, p, \mathbf{m}, \mathbf{p}, N_1, N_2, \cdots)$$

$$-S = \left(\frac{\partial G}{\partial T}\right) \qquad V = \left(\frac{\partial G}{\partial p}\right) \qquad G = U - TS + pV \tag{2.8}$$

It represents the maximum useful work that a system can do when the thermodynamic process occurs at constant temperature and pressure. From the definition of G and according with the Clausius' inequality, if the variation of Gibbs free energy during a thermodynamic process is negative, the process will be spontaneous, since it maximizes the variation of entropy in the environment [7].

According to these definitions, it is possible to define the relation that links different thermodynamic variables. In particular, if we make the derivative of each potential with respect to the relative extrinsic parameters and considering a closed system (constant N_j), we obtain the so called Maxwell relations.

$$+\left(\frac{\partial T}{\partial V}\right)_S = -\left(\frac{\partial p}{\partial S}\right)_V = \frac{\partial^2 U}{\partial S \partial V} \tag{2.9a}$$

$$+\left(\frac{\partial T}{\partial p}\right)_S = +\left(\frac{\partial V}{\partial S}\right)_p = \frac{\partial^2 H}{\partial S \partial p} \tag{2.9b}$$

$$+\left(\frac{\partial S}{\partial V}\right)_T = +\left(\frac{\partial p}{\partial T}\right)_V = -\frac{\partial^2 F}{\partial T \partial V} \tag{2.9c}$$

$$-\left(\frac{\partial S}{\partial p}\right)_T = +\left(\frac{\partial V}{\partial T}\right)_p = \frac{\partial^2 G}{\partial T \partial p} \tag{2.9d}$$

2.1.3   Thermodynamic properties of materials

The Gibbs free energy is the most useful thermodynamic potential representation for our application problem, since the differential form of G is descriptive of material properties. So, considering **B** collinear to **m** and **B** collinear to **p**, we can derive the complete differential of G:

$$dG = dU - TdS - SdT + pdV + Vdp =$$

$$= -SdT + Vdp - mdB - \mathrm{p}d\mathrm{D} + \sum_{j=1}^{N} \mu_j dN_j$$

As in the case of internal energy, is possible to describe the Gibbs free energy as the total differential with respect to the new extensive parameters. This give rise to a new set of physical relations:

$$-\left(\frac{\partial G}{\partial T}\right) \equiv S \; ; \; \left(\frac{\partial G}{\partial p}\right) \equiv V \; ; \; -\left(\frac{\partial G}{\partial B}\right) \equiv m \; ; \; -\left(\frac{\partial G}{\partial D}\right) \equiv \mathrm{p} \; ; \; \left(\frac{\partial G}{\partial N_j}\right) \equiv \mu_j \tag{2.10}$$

The material properties of a thermodynamic system can be obtained from the second derivatives of the Gibbs free energy. An interesting way to keep in compact form these properties is to define the Hessian matrix of G. The key point for this definition is to differentiate G with respect to each independent variable (the new extrinsic variables), while the other variables remain constant.

$$
\mathcal{H}(G) = \begin{pmatrix}
\dfrac{\partial^2 G}{\partial T^2} & \dfrac{\partial^2 G}{\partial T \partial p} & \dfrac{\partial^2 G}{\partial T \partial B} & \dfrac{\partial^2 G}{\partial T \partial D} & \dfrac{\partial^2 G}{\partial T \partial N} \\[2mm]
\dfrac{\partial^2 G}{\partial p \partial T} & \dfrac{\partial^2 G}{\partial p^2} & \dfrac{\partial^2 G}{\partial p \partial B} & \dfrac{\partial^2 G}{\partial p \partial D} & \dfrac{\partial^2 G}{\partial p \partial N} \\[2mm]
\dfrac{\partial^2 G}{\partial B \partial T} & \dfrac{\partial^2 G}{\partial B \partial p} & \dfrac{\partial^2 G}{\partial B^2} & \dfrac{\partial^2 G}{\partial B \partial D} & \dfrac{\partial^2 G}{\partial B \partial N} \\[2mm]
\dfrac{\partial^2 G}{\partial D \partial T} & \dfrac{\partial^2 G}{\partial D \partial p} & \dfrac{\partial^2 G}{\partial D \partial B} & \dfrac{\partial^2 G}{\partial D^2} & \dfrac{\partial^2 G}{\partial D \partial N} \\[2mm]
\dfrac{\partial^2 G}{\partial N \partial T} & \dfrac{\partial^2 G}{\partial N \partial p} & \dfrac{\partial^2 G}{\partial N \partial B} & \dfrac{\partial^2 G}{\partial N \partial D} & \dfrac{\partial^2 G}{\partial N^2}
\end{pmatrix}
\tag{2.11}
$$

According to the Schwarz theorem, the Hessian matrix is defined symmetric. So, for the sake of simplicity we reported only the upper triangular part of matrix. Using Eq.2.10 and the Maxwell relations Eq.2.9, it is possible to reduce $\mathcal{H}(G)$ as:

$$
\mathcal{H}(G) = \begin{pmatrix}
-\dfrac{\partial S}{\partial T} & \dfrac{\partial V}{\partial T} & -\dfrac{\partial m}{\partial T} & -\dfrac{\partial \mathrm{p}}{\partial T} & \dfrac{\partial \mu}{\partial T} \\[2mm]
 & \dfrac{\partial V}{\partial p} & -\dfrac{\partial m}{\partial p} & -\dfrac{\partial \mathrm{p}}{\partial p} & \dfrac{\partial \mu}{\partial p} \\[2mm]
 & & -\dfrac{\partial m}{\partial B} & -\dfrac{\partial \mathrm{p}}{\partial B} & \dfrac{\partial \mu}{\partial B} \\[2mm]
 & & & -\dfrac{\partial \mathrm{p}}{\partial D} & \dfrac{\partial \mu}{\partial D} \\[2mm]
 & & & & \dfrac{\partial \mu}{\partial N}
\end{pmatrix}
\tag{2.12}
$$

For the purpose of this representation, it is more convenient to introduce two important physical parameters: the magnetization density vector $\mathbf{M}$ and the polarization density vector $\mathbf{P}$. These parameters are defined as the collective dipole behaviour in a test volume, so they represent the global magnetic and electric properties of a system.

$$
\mathbf{M} = \frac{d\mathbf{m}}{dV} \qquad\qquad \mathbf{B} = \mu_0 \left(\mathbf{H} + \mathbf{M} \right)
$$

$$
\mathbf{P} = \frac{d\mathbf{p}}{dV} \qquad\qquad \mathbf{D} = \varepsilon_0 \mathbf{E} + \mathbf{P}
$$

where $\mathbf{H}$ is the magnetic field, $\mathbf{E}$ the electric field, μ_0 the vacuum magnetic permeability $(= 4\pi \times 10^{-7}$ H/m$)$ and ε_0 the vacuum dielectric constant $(= 8.854 \times 10^{-12}$ F/m$)$. A more detailed analysis about the magnetic properties of materials is given in Section 2.2 and Section 2.3.

If we consider an homogeneous medium, we obtain that:

$$\frac{\partial m}{\partial X_i} = V\frac{\partial M}{\partial X_i} \qquad \frac{\partial \mathrm{p}}{\partial X_i} = V\frac{\partial P}{\partial X_i}$$

Finally, from this matrix representation it is possible to extrapolate the main physical parameters associated to a generic system.

$$\mathcal{H}(G) = V\begin{pmatrix} \dfrac{1}{V}\dfrac{C_x}{T} & -\alpha_V & NK_m & NK_e & \dfrac{1}{V}\dfrac{S}{N} \\[2ex] & \dfrac{1}{V}\dfrac{\partial V}{\partial p} & -N\rho_m & -N\rho_e & \dfrac{1}{N} \\[2ex] & & -\dfrac{\chi_m}{\mu_0(1+\chi_m)} & -\dfrac{\partial P}{\partial B} & \dfrac{1}{V}\dfrac{\partial \mu}{\partial B} \\[2ex] & & & -\dfrac{\chi_e}{\varepsilon_0(1+\chi_e)} & \dfrac{1}{V}\dfrac{\partial \mu}{\partial D} \\[2ex] & & & & \dfrac{1}{V}\dfrac{\partial \mu}{\partial N} \end{pmatrix} \tag{2.13}$$

In particular C_x is the heat capacity of the system, α_V the thermal expansion coefficient, K_m the pyromagnetic coefficient, K_e the pyroelectric coefficient, ρ_m the piezo-magnetic coefficient, ρ_e the piezoelectric coefficient, χ_m the magnetic susceptibility and χ_e the electric susceptibility [8][9][10]. For the sake of simplicity, we report only the parameters useful for the analysis of the physical mechanism that are established in the CERES reactor.

$$C_x = \left(\frac{\delta Q}{dT}\right)_x = T\left(\frac{\partial S}{\partial T}\right)_x \qquad C_p = T\left(\frac{\partial S}{\partial T}\right)_p \tag{2.14}$$

$$\alpha_V = -\frac{1}{V}\frac{\partial V}{\partial T} = -\frac{1}{\rho}\frac{\partial \rho}{\partial T} \tag{2.15}$$

$$\chi_m = \frac{\partial M}{\partial H} \qquad \chi_e = \varepsilon_0\frac{\partial P}{\partial E} \tag{2.16}$$

$$K_m = -\frac{\partial M}{\partial T} \qquad K_e = -\frac{\partial P}{\partial T} \tag{2.17}$$

Note that from the matrix representation all the parameters that are multiplied by a volume factor are physical quantities associated to body forces. The other parameters are related to the time-propagation of the heat flux and the temperature. The last thermodynamic parameter that is useful to introduce is κ the thermal conductivity. It is defined starting from the **Fourier's law** [7] of heat transfer by conduction:

$$\mathbf{q} = -\kappa \nabla T \tag{2.18}$$

So, κ represents the ability to conduct heat, or better define the spatial evolution of the heat according to a variation of temperature in the material.

All the parameters that we defined are supposed to be scalar, since we defined our system as homogeneous and isotropic. If this assumption is not true, we need to pass from a scalar representation to a tensor representation, that gives the physical properties of the material according with the direction that we consider with respect to an inertial frame.

2.1.4 Magnetic Entropy and Magnetocaloric Effect

Instead of using the internal energy in order to obtain the fundamental equation, it is possible to do a similar analysis considering the entropy of a system as function of a new set of extrinsic parameters:

$$S(T, p, \mathbf{B}, \mathbf{D}, N_1, N_2, \cdots, N_r) \tag{2.19}$$

So, if we consider a closed system in which we have not a variation of the electric displacement, we will describe the entropy as the total differential with respect to the temperature T, the magnetic induction B and the pressure p:

$$dS = dS_T + dS_M + dS_p = \frac{\partial S}{\partial T}dT + \frac{\partial S}{\partial B}dB + \frac{\partial S}{\partial p}dp \tag{2.20}$$

Using this formulation, it is possible to connect directly the physical parameters of the system to the evolution of temperature and heat flux, when the system is subject to the action of an external force, as for example the force interaction due to an external magnetic field.

The Maxwell relation:

$$\left(\frac{\partial S}{\partial B}\right)_{T,p} = V\left(\frac{\partial M}{\partial T}\right)_{H,p} = \frac{\partial^2 G}{\partial T \partial H}$$

provides a smart way to connect the pyromagnetic coefficient to the entropy variation with respect to the action of a magnetic field. So, using the equations above, we obtain that:

$$dS = \frac{C_p}{T}dT + V\frac{\partial M}{\partial T}dB - V\alpha_T dp \tag{2.21}$$

If we also consider an adiabatic process ($dS = 0$), isobaric process ($dp = 0$) and $B \simeq \mu_0 H$, we reduce the previous equation from an entropy evolution of the system to a temperature variation of the system.

$$dT = -\mu_0 V \frac{T}{C_p} \left(\frac{\partial M}{\partial T} \right) dH \tag{2.22}$$

In particular, this thermodynamic behaviour is better know as **magnetocaloric effect - MCE** [11]. In fact, we can observe that an increase of magnetic field will generate an increase of temperature (and vice-versa). This effect is directly proportional to the pyromagnetic coefficient, which in turn depends on the material, the temperature and the applied magnetic field (see Sec.2.2). The MCE arises from coupling between the magnetic moments inside a material and external magnetic field, reducing the magnetic entropy S_M.

$$\Delta S_M = \mu_0 V \int_{H_1}^{H_2} \left(\frac{\partial M}{\partial T} \right) dH \tag{2.23}$$

In adiabatic processes, to compensate this loss, the temperature of the material starts to increases, until it reaches a thermal equilibrium. When the magnetic field is removed, the magnetic dipoles tend to become randomly oriented which increase the magnetic entropy and consequently the material cools down. In literature, there exist different application techniques that exploit this effect, mainly related to refrigerator machines. This effect is more evident when the system has a temperature near the Curie's temperature T_c, therefore when a ferromagnetic material lose it permanent magnet properties (due to a phase transition) it starts to be paramagnetic or diamagnetic. Hence, the pyromagnetic coefficient for a bulk ferromagnetic material, has a non-negligible value only if $T \simeq T_c$. However, it is possible to enhance K_m of materials exploiting the reduction of size in nanometer range (superparamagnetic behaviour).

$$dQ_M = T dS_M \longrightarrow \Delta Q_M = \mu_0 V T \int_{H_1}^{H_2} \left(\frac{\partial M}{\partial T} \right) dH \tag{2.24}$$

Since in our experiments MCE has a marginal role, we will not go in deeper details. Finally, it is possible to define the magnetic heat flux:

2.2 Magnetic properties of materials

2.2.1 Superparamagnetism

Magnetism is a class of physical phenomena that arise from the exchange interaction between atoms, whose origin is the requirement that electron (fermion) wavefunctions are anti-symmetric [12].

In order to minimize the Coulomb energy of the system, the wavefunction tends to keep electrons with the same spin. Thus, in the case of interacting system, the energy is lower if the electrons have parallel spins and the difference in energy between parallel and anti-parallel alignments is the **exchange energy**. This can be interpreted as a correction of the Coulomb energy required by the anti-symmetric nature of the wavefunction and produces an energy difference between anti-parallel and parallel alignment of neighbouring atomic spin moments [12]. In a simple case of two interacting atoms with spin $\mathbf{S}_1$ and $\mathbf{S}_2$, the interaction energy can be represented as:

$$E_{ex} = -J\,\mathbf{S}_1 \cdot \mathbf{S}_2$$

where J is the exchange constant, defined positive in the case of parallel allignment (favoured ferromagnetism) and negative in the case of anti-parallel allignment (favoured anti-ferromagnetism). In addition, the classical **dipolar interaction** would tend to produce an antiferromagnetic interaction, that is, the moments would be aligned anti-parallel. The exchange interaction is orders of magnitude stronger than the magnetic dipolar interactions and is the source of ferromagnetism.

Nevertheless, the dipolar interaction is the main physical mechanism involved in the formation of domains and also becomes significant in assemblies of magnetic nanoparticles, which have large magnetic moments. However, in order to reach the thermal equilibrium, the magnetostatic energy is minimized if there will exist a magnetic domain, i.e. a region within a magnetic material in which the magnetization is in a uniform direction. This is possible because of the long range nature of dipolar interaction between atoms. In fact, while the exchange interaction operates between atomic neighbours, the dipolar energy permits to minimize the energy relative to the totally magnetized state (domain), defining regions with opposite magnetization.

As with the formation of domains, there is another force that can limit the wall thickness: the **magnetocrystalline anisotropy**, i.e. the material takes more energy to magnetize it in certain directions than in others [12]. This anisotropy arises mainly from the spin-orbit interaction in the material and to the mutual interaction among the magnetic dipoles.

So, the average size of the magnetic domains depends on the three energy terms reported in Table 2.2. When the volume drops down below a critical value, it is not anymore favourable to include single-domain wall. Hence, the magnetic material below the critical size stays permanently magnetized to a value close to

Energy Term	Order of magnitude Energy per Atom (eV)	Role in Bulk Magnetic Configuration
Exchange energy	1	Responsable of ferromagentism
Magnetocrystalline anisotropy energy	10^{-3}	Limit thickness of domain walls
Magnetic dipolar energy	10^{-6}	Responsable for formation of domains

Table 2.1.   Role of magnetic energy terms.

its saturation magnetization. In this case we can state that the material is a single-domain structure. Considering a spherical particle with a uniaxial anisotropy, we obtain that the critical diameter d_c can be approximated as:

$$d_c \simeq \frac{18\sqrt{A_{ex}K}}{\mu_0 M_s^2} \tag{2.25}$$

where A_{ex} is the exchange stiffness (J m^{-1} K), K is the anisotropy energy density (J m^{-3}) and M_s is the magnetization saturation A m^{-1}. In the case of magnetite particles, $A_{ex} \simeq 10^{-11}$ J m^{-1} $K = 1.1 \times 10^4$ J m^{-3} and $M_s = 2.8 \times 10^5$ A m^{-1}, and so the critical diameter is approximately equal to 60 nm [12]. Therefore, when a ferromagnetic (or ferrimagnetic) material is defined by a diameter that is lower than its critical diameter we can say that it is in a **superparamagnetic** state.
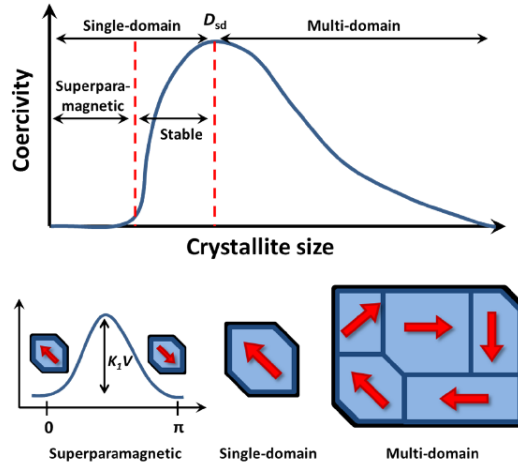
Figure 2.1.   Representation of transition from Multi-domain to Super-paramagnetic system.

This means that in a certain range of temperature, if we consider a multi-particle domain, i.e. magnetic liquid, the average magnetization in absence of an external magnetic field is zero. Also, when an external magnetic field is applied the system is able to magnetize in the same direction, similar to the paramagnetic case. This is possible because the Neél relaxation time is orders of magnitude lower with respect to the time required to measure the particles magnetization. This can be also explained taking into account the uniaxial anisotropy energy, defined as:

$$E = KV \sin^2\theta$$

where V is the particle volume and θ is the angle between the magnetisation vector and the easy axis. It is now possible to define another critical diameter as function of the temperature, at which the nanoparticle magnetization is unstable against the thermal fluctuations $KV \simeq k_B T$. Thus for a given particle size, there is a temperature that marks the transition from a permanent static moment to one that is fluctuating in a nanoparticle, i.e. T_B the blocking temperature.
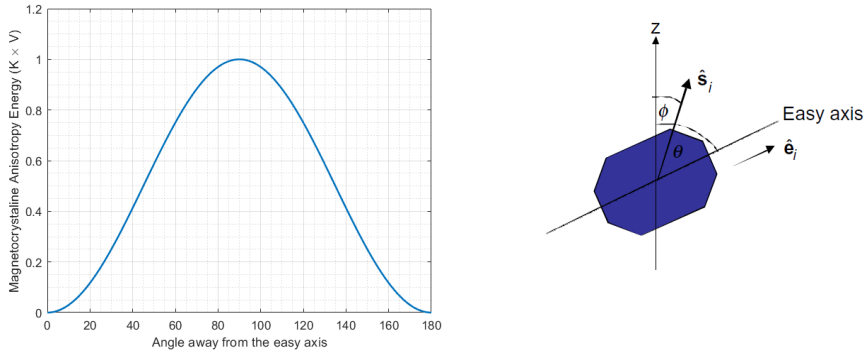
Figure 2.2.   Definition of magnetocrystalline anisotropy energy.

According to the Arrhenius law, the blocking temperature is estimated writing τ, the lifetime of the magnetization vector:

$$\tau = \tau_0 \exp\left(\frac{KV}{k_B T}\right)$$

where τ_0 is a natural lifetime or the value at the high temperature limit. In this case, the moment will appear blocked when the lifetime is longer with respect to the measurement time, that we define for example equal to 1000 s. So, the estimation can be made considering that:

$$\tau > 1000s \qquad \ln 1000 > \ln \tau_0 + \left(\frac{KV}{k_B T}\right)$$

where τ_0 is approximately equal to 10^{-9}.

$$T_B = \left(\frac{KV}{k_B \ln 10^{12}} \right)$$

In the same way, it is possible to define the blocking diameter d_{bl} at a given temperature T in the case of spherical particles:

$$d_{bl} = \left(\frac{6k_B T \ln \left(\frac{\tau}{\tau_0} \right)}{\pi K} \right)^{\frac{1}{2}} \tag{2.26}$$

Finally, a ferromagnetic material is in superparamagnetic state if at a given temperature its diameter D is below the critical diameter d_c (single-domain structure) and above the blocking diameter d_{bl} (maintain the magnetization properties):

$$\left(\frac{6k_B T \ln \left(\frac{\tau}{\tau_0} \right)}{\pi K} \right)^{\frac{1}{2}} < D < \frac{18\sqrt{A_{ex}K}}{\mu_0 M_s^2}$$

Material	Critical Diameter (nm)
Co	70
Ni	55
Fe	14
Fe_3O_4	128
γ-Fe_2O_3	166
$SmCo_5$	1500

Table 2.2.   Critical diameter of different materials [13].

2.2.2   Langevin relation and Curie's law

It is possible to describe the magnetization behaviour of a paramagnetic material according to the Langevin relation. It represents a theoretical magnetization curve as function of an external applied magnetic field in the case of ideal paramagnetic gas of particles. Hence, in this case we are not considering any dipole-dipole interaction.
The formulation is found starting from the mechanical work done on a magnetic dipole by an external magnetic field and neglecting the mutual action of the magnetization field generated by the paramagnetic particles system.

The mechanical magnetic work can be defined as:

$$W = -\mathbf{m} \cdot \mathbf{B} = -m\,B\,\cos\theta \qquad (2.27)$$

where $\mathbf{m}$ is the magnetic moment of a magnetic dipole and $\mathbf{B}$ is the magnetic induction field. The next step is to define the number density of dipoles n. According with Boltzmann statistic, the probability that a state with energy E is occupied is:

$$p_B = \exp\left(\frac{-W}{k_B T}\right) = \exp\left(\frac{m\,B\,\cos\theta}{k_B T}\right) = e^{\beta\cos\theta} \qquad \beta = \frac{mB}{k_B T}$$

It is important to note that the Boltzmann statistics says that thermal fluctuations inside our control volume counteract the action of the magnetic field. So, there is a randomness on the orientation (angular distribution) of the magnetic dipoles due to the thermal agitation of the particles. Here, we are assuming that the magnetization magnitude is constant and only its direction can change. So, it is possible to say that the tip of magnetization vector lies on the surface of a sphere, where the radius is the magnitude of $\mathbf{m}$.

The net magnetization is the average component of the total magnetization moment along the direction of the external magnetic field. Hence, supposing that the magnetic field is oriented along the z-axis, the net magnetization will be $m_z = m\cos\theta$. Therefore, from a statistical mechanics point of view, it can be defined as the ensemble average over the surface of the sphere (phase space in spherical coordinates):

$$M = n\,m\frac{\displaystyle\int_0^{2\pi} d\varphi \int_0^{\pi} e^{\beta\cos\theta}\cos\theta\sin\theta d\theta}{\displaystyle\int_0^{2\pi} d\varphi \int_0^{\pi} e^{\beta\cos\theta}\sin\theta d\theta} \qquad (2.28)$$

where $n = N/V$ is the volume concentration of magnetic dipoles, N is the number of dipoles and V is the control volume. It is possible to bring out from the integral the n contribution and m contribution since we are assuming identical and non interacting particles.

From an experimental point of view, it is better to define $n\,m$ as:

$$n\,m = \frac{N}{V}V_{NP}M_d = \Phi M_d = M_s$$

where Φ is the volume packing fraction of nanoparticles within the system ($0 \leq \Phi \leq 1$), $M_d = m/V_{NP}$ is the domain magnetization of the bulk magnetic particle, V_{NP} is the volume of the nanoparticle and M_s is the saturation magnetization, which corresponds to the value of magnetization when all dipoles are aligned with the external magnetic field. For magnetite particles $M_d = 4.46 \times 10^2$ kA/m [14]. By solving the integral, we obtain the Langevin relation:

$$M = M_s\left(\coth\beta - \frac{1}{\beta}\right) \qquad (2.29)$$

29

For sake compactness, we define the Langevin function $L(x)$ as:

$$L(x) = \coth x - \frac{1}{x} \simeq \frac{x}{3} - \frac{x^3}{45} + \cdots \qquad (2.30)$$

In the weak-field limit, the Langevin relation can be written as:

$$M \simeq M_s \frac{mB}{3k_B T} = Nm \frac{mB}{3k_B T} \qquad (2.31)$$

From a quantum mechanical point of view, the magnetic moment of a single domain structure (atom, ion, etc.) in the free space is given by:

$$\mathbf{m} = \gamma \hbar \mathbf{J} = -g\mu_B \mathbf{J} \qquad (2.32)$$

where the total angular momentum $\mathbf{J}$ is the sum of the contribution of the spin $\hbar \mathbf{S}$ and the orbital $\hbar \mathbf{L}$ angular momenta. The gyromagnetic ratio γ represents the ratio of the magnetic moment to the angular momentum and it is linked to the g-factor g, or rather the spectroscopic splitting factor, through the Bohr magneton μ_B:

$$\mu_B = \frac{e\hbar}{2m} = 9{,}27400949(80) \times 10^{-24}\ J\,T^{-1} \qquad (2.33)$$

So, according with Eq.2.31, it is possible to write the magnetization as [15]:

$$M \simeq \frac{NJ(J+1)g^2 \mu_B^2}{3k_B T} B = \frac{C}{T} B \simeq \mu_0 \frac{C}{T} H \qquad (2.34)$$

This is the well known Curie's law for paramagnetic materials, where C is the Curie's constant.
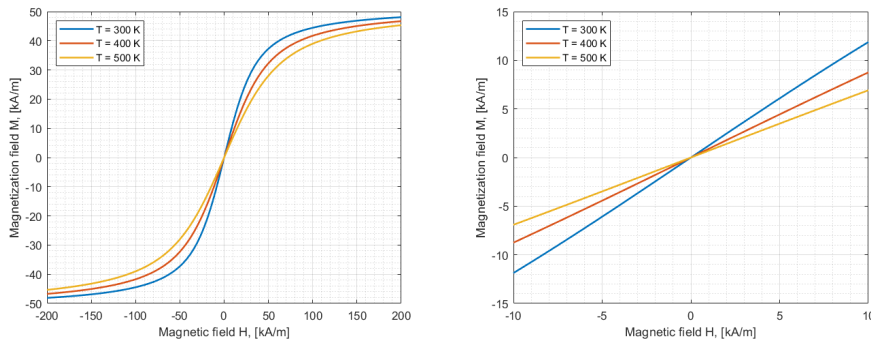
Figure 2.3. Langevin relation at different temperatures for EFH3 ferrofluid, concentration $\Phi = 0.12$. On the left side, the full magnetization curve. On the right side, the linearization in the weak field limit.

2.3   Ferrohydrodynamics

2.3.1   Governing Equations

Mass Conservation - Continuity Equation

The principle of mass conservation states that for any closed system (no transfer of energy and matter), the mass of the system must remain constant over time. In general, this concept can be associated with the definition of density, that depends both on temperature and the pressure.

$$\frac{d\rho}{\rho} = \left(\frac{\partial \ln \rho}{\partial P}\right)_T dP + \left(\frac{\partial \ln \rho}{\partial T}\right)_P dT \tag{2.35}$$

where ρ is the mass density, P the pressure and T the temperature. The first term in parentheses is the bulk compliance, while the second term is the negative of the volume coefficient of thermal expansion [16]. For our applications it is possible to neglect the finite compressibility of the fluid, since we are working far from sound wave regime. So, it is possible to consider our fluid **incompressible**, or rather there is no variation of density in time (no expansion or compression).
However, the coefficient of thermal expansion plays an important role in the dynamics of our system. So, it is possible to linearize the behaviour of the density around the temperature working point, using a first order Taylor expansion and Eq.2.15:

$$\rho = \rho_0 \left[1 - \alpha_V (T - T_0)\right] \tag{2.36}$$

where α_V is the coefficient of thermal expansion.
Using an Eulerian approach (follow a particular volume of space as the fluid moves through it [16]), it possible to demonstrate that:

$$\frac{D\rho}{Dt} + \rho \, \nabla \cdot \mathbf{u} = 0 \tag{2.37}$$

where $\mathbf{u}$ is the velocity and the term D/Dt is the material derivative, defined as:

$$\frac{D}{Dt} = \frac{\partial}{\partial t} + \mathbf{u} \cdot \nabla \tag{2.38}$$

Finally, considering that the fluid is incompressible, we obtain that:

$$\nabla \cdot \mathbf{u} = 0 \tag{2.39}$$

Momentum Conservation - Navier-Stokes Equation

The momentum equation for a magnetic fluid can be derived considering the internal and external forces acting on the fluid: in particular the different terms are

associated to inertial forces, pressure forces, viscous forces and external forces applied to the fluid, which in our case are the gravitational and magnetic ones. For an incompressible Newtonian fluid in the Eulerian frame, the momentum equation is:

$$\rho\frac{D\mathbf{u}}{Dt} = -\nabla p + \rho\mathbf{g} + \eta\nabla^2\mathbf{u} + \mathbf{f}_m \tag{2.40}$$

where ρ is the density, $\mathbf{u}$ the velocity, t the time, p the pressure, $\mathbf{g}$ the gravitational body force, η the dynamic viscosity and $\mathbf{f}_m$ magnetic body force.

It is important to note that the definition of the magnetic force is an unclear aspect of ferrofluid modelling. The most cited formulation is given by Rosensweig [17], who gave a full description for the force induced on a magnetic dipole by an external magnetic field.
In the case of dispersed paramagnetic colloidal particles, we have also to consider that the internal magnetization of the fluid induces a variation of the external magnetic field. Therefore, it is more useful for our description to lie in the fluid frame and to consider the action of the magnetic induction on the single magnetic dipole.
Using the separated magnetic charge model for a magnetic dipole[1], it is possible to evaluate the force acting on a single domain nanoparticle, represented as a magnetic dipole [18]. Therefore, the **local force** can be defined as:

$$\mathbf{F}_m = (\mathbf{m}\cdot\nabla)\mathbf{B} \tag{2.41}$$

where μ_0 the magnetic permeability, $\mathbf{m}$ the magnetization vector of a single dipole and $\mathbf{B}$ the magnetic induction, defined as:

$$\mathbf{B} = \mu_0\left(\mathbf{M} + \mathbf{H}\right) \tag{2.42}$$

The magnetization $\mathbf{M}$ represents the density of magnetic moments carried by the atoms in a material, defined as:

$$\mathbf{M}(P) = \frac{\sum_{i=1}^{N}\mathbf{m}_i}{\Delta V} \tag{2.43}$$

where ΔV is the mesoscopic volume centred in a point P and $\mathbf{m}_i$ are the atomic magnetic moments in ΔV [19]. Another possible definition can be made considering the average value of the magnetic dipole moment in an infinitesimal volume:

$$\mathbf{M} = \frac{\sum_{i=1}^{dN}\mathbf{m}_i}{dV} = \frac{dN}{dV}\langle\mathbf{m}\rangle$$

---

[1]Using Eq.2.49 it is possible to proof that the separated magnetic charge model is equivalent to the electric current loop model.

In the case of ferrofluid, the size of the dimension of the nanoparticles is below the critical diameter ($\simeq 10$ nm at 300 K [20]), so it is possible to consider the particle as a single domain structure. Therefore, $\mathbf{m}_i$ represents the magnetization of a single nanoparticle and $\mathbf{M}$ represents the magnetization density of the whole fluid. Now, it is possible to define the magnetic force per unit volume [2]:

$$\mathbf{f}_m = (\mathbf{M} \cdot \nabla)\mathbf{B} \tag{2.44}$$

In the quasi-stationary limit, the magnetized particles adjusts to the applied magnetic field almost instantly [22]. Therefore, the magnetization vector $\mathbf{M}$ will be **collinear** with $\mathbf{H}$ in each instant of time:

$$\mathbf{M} = \frac{M}{H}\mathbf{H} \qquad \mathbf{M} = \frac{M}{B}\mathbf{B} \tag{2.45}$$

Owing to these assumptions, it is possible to write:

$$(\mathbf{M} \cdot \nabla)\mathbf{B} = \frac{M}{B}(\mathbf{B} \cdot \nabla)\mathbf{B} \tag{2.46}$$

and considering the vector equality:

$$(\mathbf{B} \cdot \nabla)\mathbf{B} = B\nabla B - \mathbf{B} \times (\nabla \times \mathbf{B}) \tag{2.47}$$

Considering also a non-conducting fluid, with no displacement currents, it is possible to define the Maxwell's equations as:

$$\nabla \cdot \mathbf{B} = 0 \qquad \nabla \times \mathbf{H} = \mathbf{J} + \frac{\partial \mathbf{D}}{\partial t} = 0 \tag{2.48}$$

Using now Eq.2.42, Eq.2.45 and Eq.2.48, we obtain that:

$$\nabla \times \mathbf{B} = \mu_0 \nabla \times (\mathbf{M} + \mathbf{H}) = \mu_0 \left(\frac{M}{H} + 1 \right) \nabla \times \mathbf{H} = 0 \tag{2.49}$$

Summing up all the equations above, it is possible to write again the momentum equation as:

$$\rho \frac{D\mathbf{u}}{Dt} = -\nabla p + \rho \mathbf{g} + \mu \nabla^2 \mathbf{u} + M\nabla B \tag{2.50}$$

As defined in Sec.2.2, $\mathbf{M}$ is both function of the magnetic field and the temperature. So, it is possible to use the chain rule in order to define two important physical quantities, that characterize the fluid behaviour:

$$\nabla M(H,T) = \frac{\partial M}{\partial H}\nabla H + \frac{\partial M}{\partial T}\nabla T \tag{2.51}$$

---

[2]This term does not represent the macroscopic Kelvin body force, since it takes into account the magnetic dipole interaction, that is not negligible in ferrofluids [21].

$$\chi \equiv \frac{\partial M}{\partial H} \qquad K \equiv -\frac{\partial M}{\partial T} \tag{2.52}$$

where χ is the magnetic susceptibility and K is the pyromagnetic coefficient.
The Langevin relation and the Curie law highlight the dependence of χ with respect to the magnetic field intensity and the temperature. However, it is possible to decouple the temperature dependence using the pyromagnetic coefficient.
Hence, according with the Eq.2.34 and Eq.2.52, we might define the coefficients as:

$$\chi = \mu_0 \frac{C}{T} \qquad K = \mu_0 \frac{C}{T^2} H \tag{2.53}$$

The magnetic force per unit volume can be finally described as:

$$M\nabla B = \mu_0 M\nabla M + \mu_0 M\nabla H = \mu_0 M \left[(1+\chi)\nabla H - K\nabla T\right] \tag{2.54}$$

Considering a small variation of the magnetization around a working point, it is possible to use a first order approximation of the Taylor series to describe the intensity of the magnetization field:

$$M = M_0 + \chi\Delta H - K\Delta T \tag{2.55}$$

$$\mathbf{M} = \frac{M_0 + \chi\Delta H - K\Delta T}{H}\mathbf{H} \tag{2.56}$$

$$\Delta H = H - H_0 \qquad \Delta T = T - T_0 \tag{2.57}$$

In order to reduce the computation cost in the case of computational fluid dynamics simulations, it is possible to use the Boussinesq approximation. It assumes that variations in density have no effect on the flow field, except that they give rise to buoyancy forces. This approximation is valid as long as the variation of density is small enough $\Delta\rho \ll \rho_0$. Hence, using Eq.2.36 we obtain the complete momentum equation:

$$\rho\frac{D\mathbf{u}}{Dt} = -\nabla P - \rho_0\alpha_V\Delta T\mathbf{g} + \eta\nabla^2\mathbf{u} + \mu_0 M \left[(1+\chi)\nabla H - K\nabla T\right] \tag{2.58}$$

where P represents the pressure shift, defined as $P = p + \rho_0 g h_0$ and ρ of the inertial term is now assumed constant.

Energy conservation - Temperature Equation

Considering both thermal and mechanical energy, it is possible to evaluate the temperature equation for an incompressible magnetizable fluid. In particular, we need to combine the treatment of the electrodynamics of moving media and the thermodynamic treatment.

At first, we write the total differential for internal energy as function of entropy, magnetization and specific volume:

$$dU = TdS - pdV + \mu_0\mathbf{H} \cdot d\mathbf{I} \tag{2.59}$$

and so, for an incompressible fluid, we obtain:

$$\frac{dU}{dt} = T\frac{dS}{dt} + \mu_0\mathbf{H} \cdot \frac{d\mathbf{I}}{dt} \tag{2.60}$$

where U is the internal energy per unit mass, T the temperature, S the entropy per mass, V the specific volume, p the pressure and $\mathbf{I} = \mathbf{M}\,V$.

Following Finlayson [23], it is possible to postulate the entropy equation:

$$\rho T\frac{dS}{dt} = -\nabla \cdot \mathbf{q} + \Phi \tag{2.61}$$

where $\mathbf{q}$ is the heat flux and Φ is the viscous dissipation. Combining together the equation above and considering the continuity equation Eq.2.39, the Fourier's law for thermal conduction Eq.2.18 and the Maxwell relations Eq.2.9, we obtain the temperature equation:

$$\left[\rho C_{p,H} - \mu_0\mathbf{H} \cdot \left(\frac{\partial \mathbf{M}}{\partial T}\right)\right]\frac{DT}{Dt} + \mu_0 T\left(\frac{\partial \mathbf{M}}{\partial T}\right) \cdot \frac{d\mathbf{H}}{dt} = \kappa\nabla^2 T + \Phi \tag{2.62}$$

where $C_{V,H}$ is the heat capacity at constant volume and magnetic field and κ the thermal conductivity (assumed constant). It is important to note that in literature the pyromagnetic effect for paramagnetic particles far form their Curie's temperature are not considered in the Temperature equation. This is possible because the heat transfer due to the variation of magnetization as function of temperature represents a small percentage of the heat transfer mechanism [24]. Therefore, we suppose that conduction, natural convection and magneto-convection are the main heat transfer mechanisms in the liquid solution, neglecting the magnetocaloric effects and the viscous dissipation. So, it is possible to write the equation as:

$$\rho C_p\frac{DT}{Dt} = \kappa\nabla^2 T \tag{2.63}$$

2.3.2 Thermomagnetic convection

This phenomenon was presented for the first time by Finlayson [23], defining that it is possible to generate convection in magnetic fluids by means of spatial variation of in magnetization. This is only possible when the magnetization of the fluid depends on temperature and there is a temperature gradient across the volume containing the fluid.

In a ferrofluid system, i.e. a colloidal suspension of paramagnetic particles in a carrier liquid, the pyromagnetic coefficient can play an important role in the convection mechanism. This is only possible if the thermal gradient across a layer exceeds particular values. To understand better how the thermomagnetic convection works, we can do a simple thought experiment.

Supposing to have a one-dimensional converter, filled with ferrofluid, in which we apply an homogeneous magnetic field along the x-direction and a thermal gradient across the isothermal boundary layers of the reactor, that lays always along the x-axis.
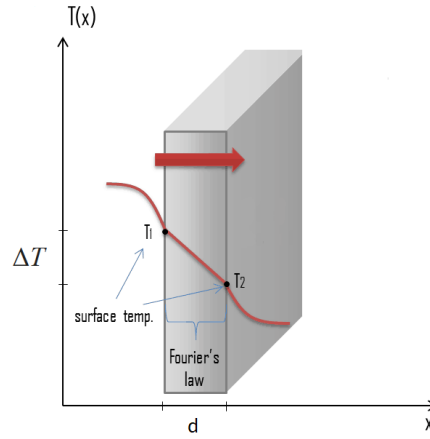
Figure 2.4.   Example of linear temperature decay in one-dimensional reactor.

Using Eq. 2.48, we know that:

$$\nabla \cdot \mathbf{H} = -\nabla \cdot \mathbf{M} \tag{2.64}$$

Furthermore, from Eq.2.64 and Eq.2.51, we obtain:

$$\frac{\partial H_x}{\partial x} = -\chi \frac{\partial H_x}{\partial x} + K \frac{\partial T}{\partial x} = \frac{K}{1+\chi} \frac{\partial T}{\partial x} \tag{2.65}$$

where H_x is the x component of the internal magnetic field. In this formulation we are saying that a spatial variation of temperature will induce a gradient of magnetic field intensity, so an induced force acting on the magnetic particles along

the x-direction. Note that the application of a constant magnetic field will not generate magnetic forces, since $\nabla H = 0$, but it is required in order to have non-null pyromagnetic coefficient (Eq.2.53).

After that, if we also suppose that the distance between the isothermal layers is small enough, we can consider the thermal gradient as linear. Therefore, it is possible to write the previous equation as:

$$H(x) = H(0) + \frac{K}{1+\chi} \frac{\Delta T}{d} \, x \qquad (2.66)$$

where $H(0)$ is the value of the external magnetic field intensity. Finally, we understand that the crucial term that can increase the effect of the thermo-magnetic force is the difference of temperatures across the layers ΔT and the distance between the layers d, so the geometry.
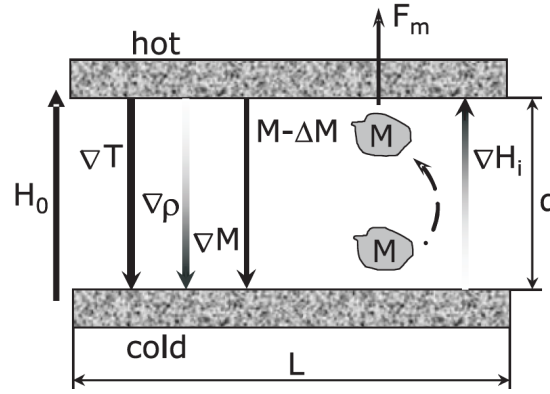
Figure 2.5. Sketch of the explanation of thermomagnetic effect [22].

So, the thermomagnetic convection is the result of the ponderomotive force due to non uniform magnetization. As in the case of natural convection, this phenomenon arises as consequence of non uniform heating, but in the buoyancy case the force components is associated to a variation of the fluid density along the gravity direction. Instead, the body force associated to the thermomagnetic convection lies along the direction of the thermal gradient.

One of the most important application of nonconducting ferrofluid is to exploit the relatively high pyromagnetic coefficient, even far from its Curie's temperature, to induce a thermomagnetic convection in the case of reduced gravity conditions, as for example on orbital stations. This permits to increase the heat exchange efficiency when the cooling by natural convection cannot be achieved [25].

Finlayson [23], in his analysis, provides numerical results that highlights that convection can be induced as spatial variation in magnetization of the fluid, depending

on the temperature and the temperature gradient established across the layer. In thin layers ($\leq 1mm$), magnetic convection predominates over the buoyancy mechanism.

	ΔT (°C)					
	Water		Kerosene		n-Heptane	
d (cm)	Buoyancy alone	Buoyancy and magnetic	Buoyancy alone	Buoyancy and magnetic	Buoyancy alone	Buoyancy and magnetic
1	0.1	0.1	0.05	0.05	0.008	0.008
0.5	0.9	0.9	0.4	0.4	0.06	0.06
0.2	15	7	6	5	1	1
0.1	120	17	51	19	8	5

Table 2.3. Temperature difference required to induce convection in magnetite-based ferrofluid [23]

2.3.3 Thermomagnetic advection

We have seen that the thermomagnetic convection can be an interesting way in order to increase the heat exchange in fluid media. However, the force interaction along the thermal gradient direction can be a good solution to impose a defined direction in the case of thermally activated motion for magnetic fluids.

$$\mathbf{f}_b = -\alpha_V \, \Delta T \, \mathbf{g} \qquad \mathbf{f}_m = \mu_0 M (1 + \chi) \nabla H - \mu_0 M K \nabla T$$

So, in the case of the motion of ferrofluid, it is more properly correct to talk about of thermomagnetic advection, where it is possible to define convection motion along different directions: the buoyancy component is always along the gravity vector direction, while the magnetic force follows the gradient of the external magnetic field and the thermomagnetic convection component lies on the direction defined by the gradient of the temperature.

Suslov et al. [25] proposed a computational and experimental analysis in a vertical layer geometry, in which they considered a kerosene-magnetite based ferrofluid. In order to observe the direct action of the magnetoconvection, they imposed the front and back layer as isothermal surfaces, in which it was possible to fix the thermal gradient. Furthermore, an homogeneous and isotropic magnetic field codirected with respect to the thermal gradient vector was imposed using an Helmholtz coil. The results show different possible motions of the liquid solution, that changes strongly according with the magnitude of the magnetic field and the intensity of thermal gradient. In particular, they defined four types of characteristic motions, that are reported in Fig.2.6.
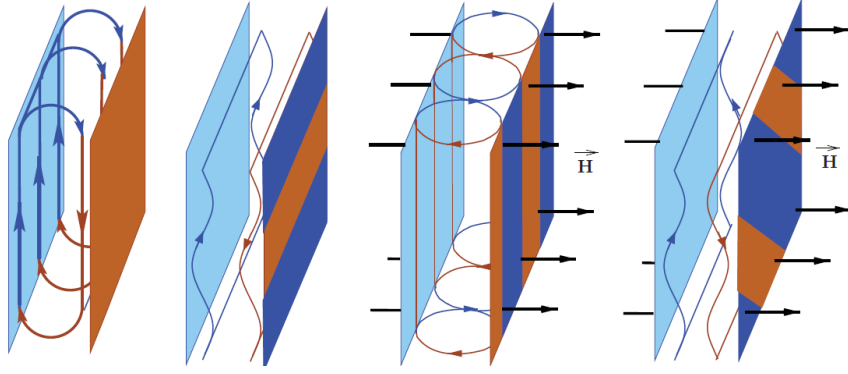
Figure 2.6.   Schematic diagram of main flow patterns (from the left to the right): basic flow; thermogravitational waves; stationary vertical thermomagnetic rolls; oblique thermomagnetic waves [25].

These particular fluid motions are associated to different simulations, where the temperature gradient and the magnitude of the magnetic field was changed according with the geometry of the system. In the case of the CERES system it is possible to exploit the different characteristics of the proposed motions, in order to generate a periodic flow along the toroidal axis of the tank. The most suitable solution for our purposes is to define a geometry in which the gradient of temperature can guarantee a natural convection component, while the thermomagnetic effect defines a concatenated stationary vertical themomagnetic rolls. The combination of the two effects defines a spiral-like motion and so, a thermomagnetic advection.

2.4 Magnetic flux in CERES system

The idea behind the CERES system is to recover electrical energy from a low enthalpy thermal gradient. It is mainly done converting the momentum generated by the motion of a magnetic fluid in electro-magnetic energy. This mantra differs completely from today's market solutions, since in this case there is not a direct conversion mechanism from thermal energy to electric power, but it can be described as a two-phase recover mechanism: the first one is the thermally driven motion generation and the second is the electromagnetic harvesting. So, the main goal is to define a thermally activated velocity variation in a periodic closed system (the tank). However, the liquid motion can be produced in different ways, from a themomagnetic advection to a mechanically driven mechanism.

The extraction system is based on the Faraday-Neumann-Lenz law, in which a variation in time of the magnetic induction flux over an open surface will generate an induced electromotive force.

$$\phi_m(t) = -\frac{\partial \Phi(\mathbf{B})}{\partial t} = -\frac{\partial}{\partial t} \iint\limits_{\Sigma(t)} \mathbf{B}(\mathbf{r}(t)) \cdot \hat{n} \, dS \tag{2.67}$$

According to the linearity of the derivative and integral operators, it is possible to decouple the time variation with respect to the magnetic induction (transformer) and the open surface (motional) [3].

$$\phi_m(t) = -\left(\left.\frac{\partial \Phi(\mathbf{B})}{\partial t}\right|_{\Sigma=const} + \left.\frac{\partial \Phi(\mathbf{B})}{\partial t}\right|_{\mathbf{B}=const} \right) \tag{2.68}$$

$$\phi_m(t) = -\underbrace{\iint\limits_{\Sigma} \frac{\partial \mathbf{B}(\mathbf{r}(t))}{\partial t} \cdot \hat{n} \, dS}_{\text{Transformer}} + \underbrace{\oint\limits_{\partial\Sigma} \mathbf{v}_\Sigma(\mathbf{r}(t)) \times \mathbf{B}(\mathbf{r}(t)) \, \vec{dl}}_{\text{Motional}} \tag{2.69}$$

On the one hand, the tranformer part of the integral represents the power generated by the variation of particle magnetization in time, defined in a fixed region Σ. On the other hand, the motional part can represents the effects of the surface motion or the surface deformation in time. The motional electromotive force represent the action of the Lorentz force on the free charges (electrons) in the conductive material that defines the open surface. Note that this effect can be observed only if the charges have a velocity component with respect to the magnetic induction field. Therefore, the velocity term represents the variation in time of the open surface Σ along a generic path.

---

[3]The full mathematical treatment that can explain the expansion of the magnetic flux derivative Eq.2.69 can be found in [26].

So, if we suppose to have a static magnetic field, completely differentiable and defined in each point of the domain, the magnetic induction will be defined as:

$$\mathbf{B}(\mathbf{r}(t)) = \mu_0 \left[\mathbf{H}(\mathbf{r}) + \mathbf{M}(\mathbf{r}(t))\right] = B(\mathbf{r}(t)) \, \hat{u}_B$$

where $\hat{u}_B$ is the $\mathbf{B}$ unit versor. Note that the expression $(\mathbf{r}(t))$ represents the functional of the magnetic induction, described through the displacement vector. The first term in the transformer part is a derivative of a vector field with respect to a scalar term. So, it is possible to develop this term as:

$$\frac{\partial \mathbf{B}}{\partial t} = \frac{\partial B}{\partial t} \hat{u}_B + \boldsymbol{\omega}_B \times \mathbf{B} \tag{2.70}$$

where $\boldsymbol{\omega}_B$ is the angular velocity of the vector $\mathbf{B}$. Considering that the magnetic induction field will be oriented along the normal vector of the surface in order to maximize the magnetic flux $(\hat{u}_B \cdot \hat{n} = 1)$, we can say that:

$$(\boldsymbol{\omega}_B \times \mathbf{B}) \cdot \hat{n} = 0$$

Since we are supposing to have a static external magnetic field, the time derivative of the magnetic induction is:

$$\frac{\partial B}{\partial t} = \mu_0 \frac{\partial M}{\partial t} \tag{2.71}$$

At last, the CERES system is designed to harvest energy using static coils that define a static open surface Σ. So, the motional part of the equation can be neglected. We can sum up all the equations to obtain a compact form for the time definition of the electromotive force $\phi(t)_m$:

$$\phi_m(t) = - \iint_\Sigma \mu_0 \, \frac{\partial M(\mathbf{r}(t))}{\partial t} \, \hat{u}_B \cdot \hat{n} \, dS \tag{2.72}$$

It is now possible to use the chain rule in order to reduce the variation of the scalar field M into its spatial and temporal components:

$$\frac{\partial M(\mathbf{r}(t))}{\partial t} = \nabla M(\mathbf{r}) \cdot \mathbf{v}_p(t) \tag{2.73}$$

where $\mathbf{v}_p(t)$ is the particle velocity distribution as function of time and $\nabla M(\mathbf{r})$ is the gradient of the magnetic induction. Note that all the parameters are defined only in the integral domain Σ. The closed-form equation can be now described as:

$$\phi_m(t) = - \iint_\Sigma \mu_0 \left[\nabla M(\mathbf{r}) \cdot \mathbf{v}_p(t)\right] \left[\hat{u}_B \cdot \hat{n}\right] dS \tag{2.74}$$

The magnetization field can be defined according with the Langevin relation Eq.2.29, so the temperature, the magnitude of the external magnetic field and the particle concentration play a fundamental role. It is also important to take into account that all these parameters influence the motion generation part of the system.

It is possible to extend the domain of integration using a solenoid coil structure for the harvesting. In this way, we can define a "volumetric domain", where ϕ_m is proportional to the number of coil of the solenoid N:

$$\phi_m(t) = -\sum_{i=1}^{N} \iint_{\Sigma_i} \mu_0 \left[\nabla M(\mathbf{r}) \cdot \mathbf{v}_p(t) \right] \left[\hat{u}_B \cdot \hat{n}_i \right] dS \tag{2.75}$$

If we suppose that the magnetization and velocity contribution is equal along the solenoid, we can rewrite the previous equation as:

$$\phi_m(t) = -N \iint_{\Sigma} \mu_0 \left[\nabla M(\mathbf{r}) \cdot \mathbf{v}_p(t) \right] \left[\hat{u}_B \cdot \hat{n} \right] dS \tag{2.76}$$

It is interesting to note that the electromotive force is generated by the variation of the relative magnetic permeability, or rather by the movement of the ferromagnetic core inside a solenoid.

One simple approximation that can be done is to suppose that the magnetization field is parallel to the normal surface vector, the velocity of the particles is collinear with respect to the gradient of the magnetic induction and M is a symmetric function with respect to the centre of the solenoid. In this way it is possible to reduce the Eq.2.76 as:

$$\phi_m(t) = -N \, \mu_0 \, \frac{\Delta M}{L} \Sigma v_p(t) \tag{2.77}$$

where $\langle M \rangle$ is the mean value of the magnitude of the magnetization along the length of the solenoid, L is the length of the solenoid and Σ is the area of the solenoid. The term $n = N/L$ is usually called linear coil density. If we also are in the weak-field limit and the temperature is assumed constant, using Eq.2.34 we obtain a compact form for the electromotive force:

$$\phi_m(t) = -n \, \mu_0 \, \frac{C}{T} \, \Delta H \, \Sigma \, v_p(t) \tag{2.78}$$

Now, it is more clear that in order to define the best design of the CERES reactor, we should know how the velocity changes according with the temperature and the magnetic field $\mathbf{v}_p(T, \mathbf{H})$. This can be done either with an olistic approach, mainly based on the experimental knowledge of the physical mechanisms that are involved in the motion generation, or simulating the behaviour of the fluid inside the tank. However, one important consideration that can be done is to characterize the extraction system in a controlled way, for example forcing the velocity magnitude and direction through a mechanical pump.

2.5   Triboelectric Effect

The triboelectric effect can be defined as a contact-induced electrification in which a material becomes electrically charged after it is physically dose to with a different material through friction [27]. It is possible to have experience about this effect in everyday life, since it is the cause of electrostatic phenomena. Although it is most frequently experienced, the mechanism behind the triboelectrification is still under debate, since there exist a solid-state approach to explain it or a more olistic approach, mainly based on a engineering modeling.

When two different materials come into contact, a chemical bonding is established between the surfaces of the materials (adhesion) and if the process is slow enough, there is a charge flow in order to reach the thermal equilibrium. This implies that the electrochemical potential of the two materials becomes equal. This charge transfer can be made by electrons, holes or by ion/molecules. The sign of the charges to be carried by a material depends on its relative polarity in comparison to the material to which it will contact [27]. Using energy band diagrams, it is possible to illustrate the case of triboelectrically negative dielectric material that exchange electrons with a metal structure.
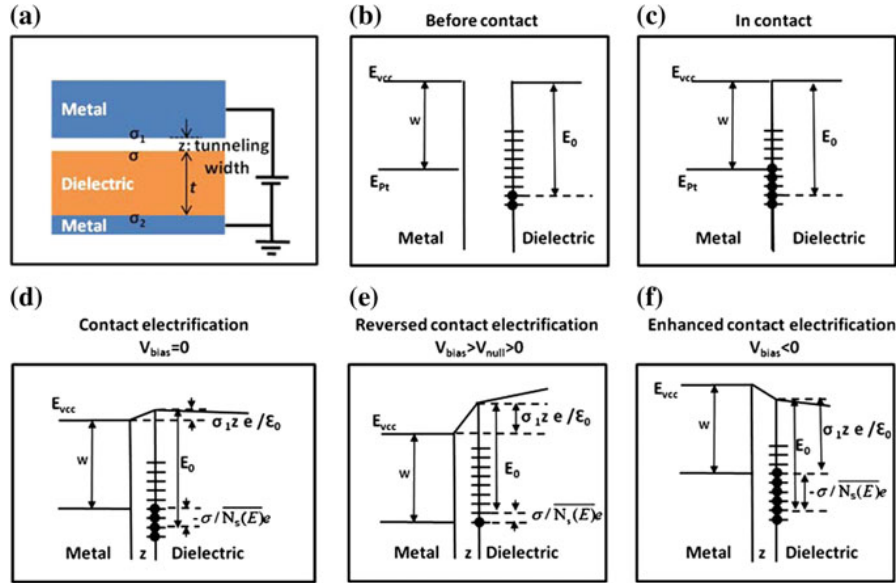
Figure 2.7.   Schematic of a triboelectric process. **a**) Model of the device. **b**) Energy band diagram of a metal and a dielectric material before the contact. The energetic states in between the conduction and the valence band represent defects on the structure or the HOMO-LUMO levels in a polymeric material. **c**) and **d**) Representation of the thermodynamic equilibrium. **e**) and **f**) Deformation of the energy levels due to the application of an external voltage bias [27].

During the separation process, some of bonded atoms have the tendency to keep electrons, mainly due to the difference of electronegativity between the two materials, and this produces a charge accumulation on the surfaces. Furthermore, the active area plays an important role, since the process is highly related on the friction coefficient.

In order to maintain this charge, the characteristic time of discharge can be modeled as an RC circuit $\tau = 1/RC$, so the choice of material is defined according to high resistivity and high relative dielectric constant (good electric insulator), the geometrical parameters, high difference in electronegativity and high active surface. Almost any material we know undergoeas the triboelectrification effect, synthetic polymers, to metals, to wood and silk. However, the ability of a material for losing/gaining electron depends on its polarity, so the choice of materials is strongly dependent on the application in which they are involved in [27]. This tendency to gain or lose electrons is usually described using the so called triboelectric series.

Positive		Negative
	Aniline-formol resin	Polyvinyl alcohol
	Polyformaldehyde 1.3-1.4	Polyester (Dacron) (PET)
	Etylcellulose	Polyisobutylene
	Polyamide 11	Polyuretane flexible sponge
	Polyamide 6-6	Polyethylene terephthalate
	Melanime formol	Polyvinyl butyral
	Wool, knitted	Formo-phenolique, hardened
	Silk, woven	Polychlorobutadiene
	Polyethylene glycol succinate	Butadiene-acrylonitrile copolymer
	Cellulose	Nature rubber
	Cellulose acetate	Polyacrilonitrile
	Polyethylene glycol adipate	Acrylonitrile-vinyl chloride
	Polydiallyl phthalate	Polybisphenol carbonate
	Cellulose (regenerated) sponge	Polychloroether
	Cotton, woven	Polyvinylidine chloride (Saran)
	Polyurethane elastomer	Poly(2,6-dimethyl polyphenyleneoxide)
	Styrene-acrylonitrile copolymer	Polystyrene
	Styrene-butadiene copolymer	Polyethylene
	Wood	Polypropylene
	Hard rubber	Polydiphenyl propane carbonate
	Acetate, Rayon	Polyimide (Kapton)
	Polymethyl methacrylate (Lucite)	Polyethylene terephtalate
	Polyvinyl alcohol	Polyvinyl Chloride (PVC)
	(continued)	Polytrifluorochloroethylene
		Polytetrafluoroethylene (Teflon)

Figure 2.8. Triboelectric series [27].

After the choice of the materials in the triboelectric series, the morphology of the surfaces can be modified by physical and chemical techniques with the creation of

nano-patterns, which are effective for enhancing the contact area and possibly the triboelectrification.
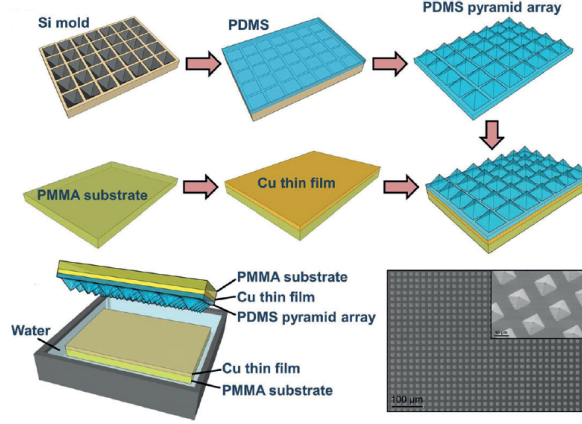
Figure 2.9.   Example of pyramid nano-pattern for triboelectric device [28]

Furthermore, the surface of the material can be chemically functionalized using nanoparticles, molecules, nanotubes or nanowires to enhance the triboelectrification process changing the surface potential and the local contact characteristics.

2.5.1   Single-Electrode Mode

Recently, with the advent of low power electronics (recovery systems, envirnomental monitoring, IoT etc.), the triboelectric devices have found employment as a renewable energy source, since it is possible to harvest energy from numerous types of mechanical energy, including vibrational, rotational, wind and tidal wave energy. The important characteristics of these devices consist in their ease of fabrication, stability and high-energy conversion efficiency [29]. So, the right functionalization of a triboelectric nanogenerator (TENG) is important in order to build a marketable device for recovery applications.
TENG has four basic modes of operations, that can be used in different operating conditions, according to the specific application. This modes are represented in Fig.2.10 and for sake of simplicity we reported only a detailed explanation of the Single-electrode Mode (SETENG) devices, that is mainly used in this thesis project.

Differently from the other cases, the SETENG presents only one electrode connected to a load. This is fundamental for mobile applications, such as human walking on the floor or to recover energy from the friction generated by the motion of a fluid, where we have only one movable object. The other electrode is just a reference, that can be placed anywhere in the space, but in the case of device characterization is usually directed to the same ground of the measurement systems [27].
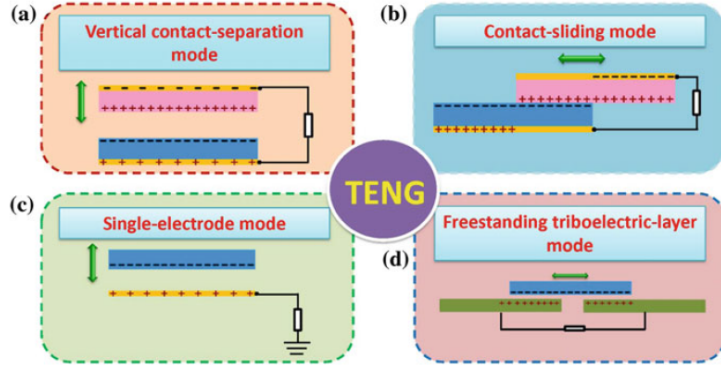
Figure 2.10. Device operation of a Triboelectric Nanogenerator (TENG). **a**) Vertical contact-separation mode. **b**) Contact-sliding mode. **c**) Single-electrode mode. **d**) Freestanding triboelectric-layer mode [27].

The operating principle can be described by the coupling of contact electrification and electrostatic induction. Taking into account a conductor-to-dielectric system it is possible to do a simple analysis of the physical phenomenon. For example, an alluminum primary electrode is brought into contact with a fluorinated ethylene propylene (FEP) and surface charge transfer takes place on the contact area of the two materials. Considering the triboelectric seris, the FEP have a tendency to accumulate electrons due to the presence of fluorinated groups (high electronegativity), and a net positive charges are transferred on the alluminum surface. Considering the insulating properties of the polymers, there will be a long-time retention of triboelectric charges (hours or even days) [27]. Now, considering a reference electrode, a potential difference is established between the two electrodes. The open circuit voltage V_{OC} keep increasing until reaching the maximum value. Finally, when a load is attached in between the two electrodes, there will be a presence of an instantaneous current. This effect can be observed or if there is a continuous contact-separation between the two materials (contact mode) or if there is a continuous charge accumulation because of a flowing medium, as in the case of water-based applications [27].

2.5.2 Where is water in the triboelectric series?

Water plays an important role in the electrification of materials. A particular kind of contact electrification (flow electrification) has been reported in different studies [30] [31], where insulating liquids cause electrification of electronic components or determines shock problems in petroleum pipeline hazards. However, other interesting triboelectric characteristics can be associated to pure water flowing through

hydrophobic surfaces, such as polytetrafluorethylene (PTFE). The key point in order to understand how is it possible to exchange charges in a water solution is to determine where is water in the triboelectric series.

An interesting analysis provided by Burgo et al.[32] gives a complete outlook on the electrification processes in pure water. In particular, ion-partitioning near solid-liquid interfaces (hydroxil adsorption of water-hydrophobic surfaces) is fundamental in material electrification.

At hydrophobic interfaces, hydroxyl ions are predominantly adsorbed at the Stern layer causing negative electrification. Also, the exclusion-zone (EZ) formed on the vicinity of various hydrophilic surfaces displays a negative net charge while balanced by complementary positive charge beyond the EZ, formed by protons or hydronium ions in the bulk of water. The difference of magnitude between materials tested must be due to the ability of each material to adsorb $[OH(H_2O)_n]^-$ ions or to produce larger or thinner EZ charged interfaces.
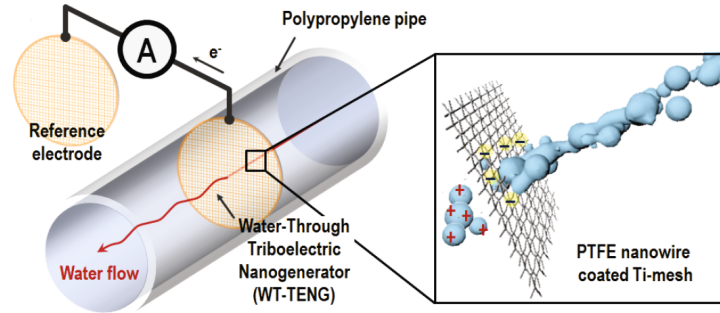
Figure 2.11. Example of water-based triboelectric effect using a Ti-mesh, in Single Electrode Mode [29].

The idea behind this thesis project is to exploit the positive charging of water in a FEP pipe (negative material in the triboelectric series) in order to have an accumulation of electrostatic energy from the fluid motion, that is generated by wasted sources. Inspired by the work of Ravelo et al.[33], we built a simple experimental setup to characterize the triboelectric effect in a water-based colloidal solution. The modeling of the device was done considering an RC circuit, where the resistive component was associated to the conductivity of the solution, the capacitive component to the geometrical properties of the electrodes and to the insultaing properties of the polymer interface and finally, the current flowing in the electrodes proportional to the velocity in the pipe. A detailed analysis is provided in the Sec.6.

Chapter 3

Colloidal Systems

The colloid is a complex condensed matter system lying at the boundary between completely homogeneous systems such as solutions and completely heterogeneous systems such as suspensions [34]. It is usually defined as a stable suspension of nanoparticles in a carrier fluid, that can be in liquid or gas form. They are classified according to the aggregation state of their components, the dispersant (carrier phase) and the dispersoid (suspended phase).

These fluids are characterized by a suspended phase with the ability to confer specifically physical properties according with the nature of the nanoparticles (magnetic, thermal, photo, etc.), maintaining the liquid nature of the solution. The other advantage is that in the limit of stability, the global system can be considered as single-phase, since the mutual interaction among the particles and the molecules of the carrier liquid are balanced by the Brownian motion (induced by the thermal effects) and by the physico-chemical properties of a dispersant. However, colloids feature non-trivial collective properties and can present some phase transitions: for instance flocculation, occurring when the dispersoids coalesce, gelation, occurring when the dispersant changes viscosity and Coulomb explosion. Those phase transformations can be reversible, and can also depend on an exogenous input for that reversibility to occur [34].

3.1 Stability

One of the most important feature associated to colloidal systems is the homogeneity of the samples, or rather to keep the nanoparticles evenly dispersed in a carrier fluid. If we consider a generic system in which an external magnetic field, the gravity and the Van der Waals forces (attraction forces among nanoparticles) tend to destabilize the suspension by agglomeration or sedimentation, there are two main effects that can guarantee the stability of the system: the Brownian motion, i.e. the random movement of fine particles in a carrier liquid and the steric or the ionic

repulsion. These effects permit to keep the particles spaced and in suspension. Therefore, it is possible to say that a colloidal system is in stable state if there is a balance of the energies associated to the stabilizing and destabilizing mechanisms. In particular, from the equipartition theorem (model of vibrational energy of colloidal harmonic oscillator) it is possible to define the thermal energy associated to a spherical particle in colloidal suspension as [14]:

$$E_T = k_B \, T \tag{3.1}$$

where k_B is the Boltzmann constant (1.38×10^{-23} m^2 kg s^{-2} K^{-1}) and T is the temperature. To provide sufficient mixing is it simply necessary that the gravitational energy or the magnetic energy is lower than the thermal energy.

3.1.1 Gravity

The thermal energy is the expression of the Brownian motion that permits to the nanoparticles to move freely from the bottom to the top of the solution. In order to study the effect of sedimentation due to gravitational effects, it is necessary to define the difference of potential energy ΔE_p associated with the reduced weight (sum of the Archimedes forces and the gravity) of a nanoparticle, between the bottom and the top of the solution:

$$\Delta E_p = (\rho_p - \rho_{bf}) \, Vgh \tag{3.2}$$

where ρ_p is the density of magnetic nanoparticles, ρ_{bf} is the density of the base fluid (solvent), V is the volume of the particle, g is the standard gravity constant and h is the relative height. As we introduced before, we consider the nanoparticle with a spherical shape. So, the volume can be described as function of the diameter D:

$$V = \frac{\pi D^3}{6} \tag{3.3}$$

Finally, it is possible to define the critical diameter, i.e. the maximum diameter that the particle can have in order to be in a stable state due to gravitational effects.

$$E_T > E_p \qquad D < \left(\frac{6k_B T}{\pi \left(\rho_p - \rho_{bf} \right) gh} \right)^{\frac{1}{3}} \tag{3.4}$$

3.1.2 Magnetic field

The other sedimentation effect is the one generated by the action of an external magnetic field. Following the same procedure, it is possible to define the magnetic potential energy as:

$$E_H = -\mathbf{m} \cdot \mathbf{B} \tag{3.5}$$

In order to move the magnetic particle, it is necessary to have a difference of magnetic field intensity inside the solution. Hence, we can define a variation of potential energy ΔE_H that is proportional to the difference of the magnetic field intensity. Supposing that the magnetization is collinear to the external magnetic field, we obtain that:

$$\Delta E_H = -\mu_0 m \Delta H \tag{3.6}$$

The intensity of the magnetic moment is:

$$m = M_d V_{NP} = \frac{\pi M_d D^3}{6} \tag{3.7}$$

where M_d is the domain magnetization of the constitutive material. For magnetite-based ferrolfuids this value is $M_d = 4.46 \times 10^2 \, kA/m$ [14].
In this case, the critical diameter is equal to:

$$E_T > \Delta E_H \qquad D < \left(\frac{6 k_B T}{\pi \mu_0 M_d \Delta H} \right)^{\frac{1}{3}} \tag{3.8}$$

3.1.3   Magnetic dipole

The other important effect that induces instability inside the system is the agglomeration of the nanoparticles. Basically, it must be avoided to reduce the effect of sedimentation and to guarantee the homogeneity in the solution. This is a clue point for the fluid dynamic behaviour of the system, since the magnetic colloids (ferrofluid) can change its viscosity according with the application of an external magnetic field. These magnetoviscous effects are dependent on the magnetic dipole-dipole interaction.
The approach to study this interaction is similar to the one proposed in the applied magnetic field case. Now, we consider the movement of one nanoparticle in the magnetic field generated by the other one. In order to minimize the potential energy, the two particles tend to get closer.
So, the dipole-dipole energy E_{dd} can be expressed as:

$$E_{dd} = -\frac{\mu_0}{4\pi} \left(3 \frac{(\mathbf{m}_1 \cdot \mathbf{r})(\mathbf{m}_2 \cdot \mathbf{r})}{r^5} - \frac{\mathbf{m}_1 \cdot \mathbf{m}_2}{r^3} \right) \tag{3.9}$$

where $\mathbf{r} = \mathbf{r}_1$ - $\mathbf{r}_2$, that are the distance vectors with respect to the center of gravity.

Assuming that the two particles are close enough to guarantee the collinearity, they reach the minimum of energy when they are in contact. Therefore, replacing D instead of r and $M_{s,p}$ as magnetic dipole intensity and using Eq. 3.7, we obtain:

$$E_{dd}^{min} = -\frac{\pi \mu_0 M_d D^3}{72} \tag{3.10}$$
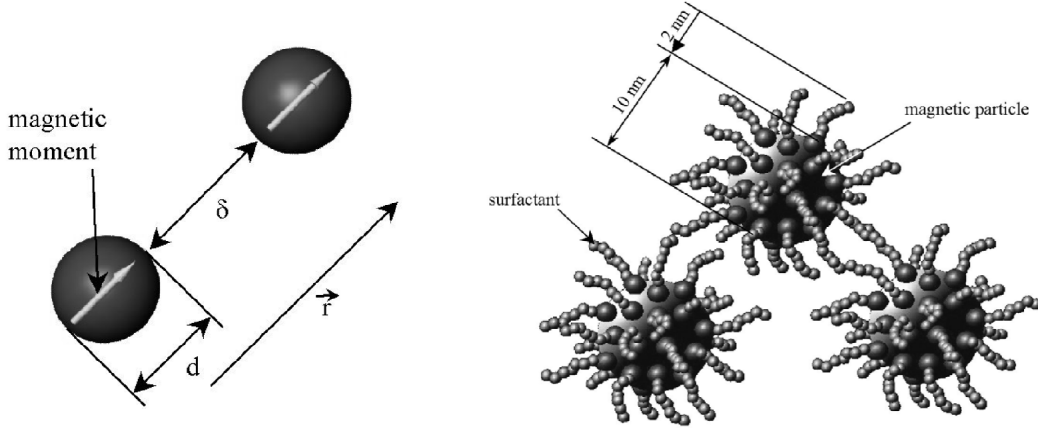
Figure 3.1. Representation of magnetic particles and relative magnetic dipole moment interaction [14].

The stability condition is defined considering the thermal energy of two nanoparticles:

$$2E_T > |E_{dd}^{min}| \qquad D < \left(\frac{144 k_B T}{\pi \mu_0 M_d^2} \right)^{\frac{1}{3}} \tag{3.11}$$

3.1.4 Electrostatic interparticle forces

Colloidal particles in a suspension experience forces as result of two force mechanisms: attractive electrostatic dipole-dipole interactions, i.e. Van der Waals forces, and repulsive electrostatic forces that arises from the interaction of electric double layer. There is also another effect, a repulsive force among adsorbed molecules on the surface of the particles, also known as steric force [35]. It is possible to exploit these effects to avoid agglomeration, using different techniques based on: adjusting the solution pH and the ion concentration and using surfactants or polymers that adsorb on particle surfaces.

The Van der Waals forces are essentially interactions among particles separated by any medium. In general, different materials experience this interaction only if they are in close contact, since the interaction energy is inversely proportional to the sixth power of the separation distance. There exist three different types of molecular or atomic interactions: Keesom interaction, Debye interactions and London dispertion forces. In particular, the Debye interactions are defined as the attractive energy between a non-polar molecule and a polar molecule, the Keesom arises from permanent dipole to permanent dipole interactions, while the London forces are generated by the induced dipoles arising from electronic polarization of interacting atoms (i.e. induced dipole-dipole interaction).
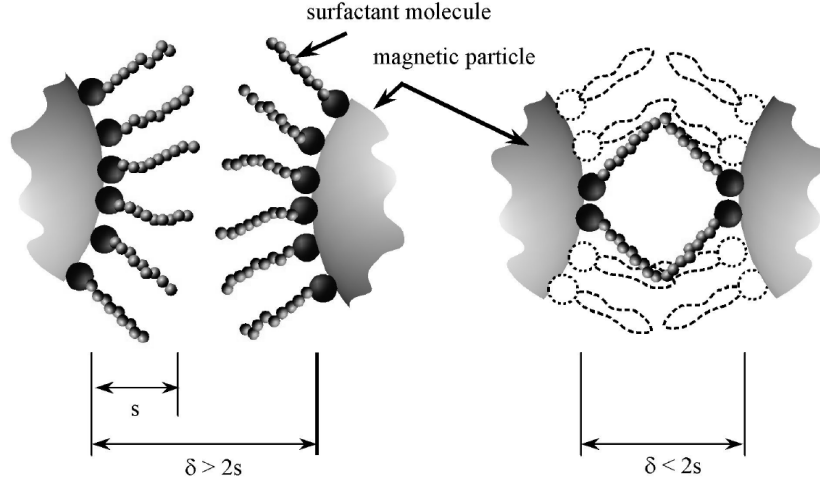
Figure 3.2.   Surfactant action in oil-based colloids [14].

If we consider also this case, the Van der Waals interactions between identical spherical particles with diameter D, it is possible to model the interaction energy according to Hamaker results [36]:

$$E_{VdW} = -\frac{A}{12}\left[\frac{1}{x^2+4x} + \frac{1}{(x+2)^2} + 2\ln\left(\frac{x^2+4x}{(x+2)^2}\right)\right] \qquad (3.12)$$

where A is the Hamaker constant, and it proportional to the the number density of the interaction particles [1]. However, x represents a distance parameter, proportional to the separation distance δ (i.e. the distance between the surfaces of the particles) and it is equal to:

$$x = \frac{2\delta}{D}$$

From this formulation it is evident that if the particles are in close contact ($x = 0$), the interaction energy tends to infinity. So, the thermal energy can not be the physical mechanism that can provide stability against the agglomeration.
Depending on the chemical nature of the solvent, it is possible to exploit either the electrostatic repulsion or the steric repulsion to guarantee stability in the solution.

---

[1]The Lifshitz theory of Van der Waals forces provides a more complete dissertation, in which it takes into account the interaction between every pair of molecules located in the two bodies, rather than treating each pair independently [37].

Water-based colloid In the case of polar medium, such as water, electrostatic forces are present due to the interaction of the charged particles and the solution. The system can be considered globally neutral, therefore the surface charge of the particle is compensated by absorbed ions chemically bonded to surface sites in the region immediately next to the surface [35] . This layer is also known as Stern layer and the electrostatic accumulation of the counterions is generally define as electrical double layer.
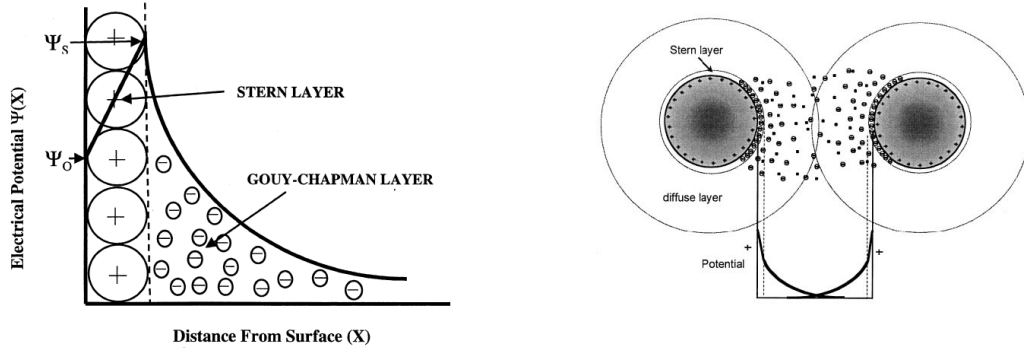
Figure 3.3. Example of Stern Layer in a spherical particle system [35].

This charge density gives rise to a surface potential, that for a spherical particle can be described as:

$$\Psi(\mathbf{r}) = \Psi_s \, e^{-\kappa \mathbf{r}} \tag{3.13}$$

where κ is the inverse Debye length, that for a chemical solution is equal to:

$$\kappa^{-1} = \sqrt{\frac{\varepsilon k_B T}{e^2 \sum c_i z_i^2}} \tag{3.14}$$

where e is the electron charge, ε the dielectric constant and c the concentration of ions with valence z.
By solving the Poisson-Boltzmann equation, considering identical spherical particles and low Stern potential Ψ_s, we obtain the interaction energy $W_{EI}(D)$ as function of surface separation distance δ:

$$E_{ei}(X) = \pi \varepsilon D \Psi_s^2 e^{-\kappa \delta} \tag{3.15}$$

With respect to previous cases, the dimension of the nanoparticle defines the separation distance. This is mainly due to the fact that there is a minimum in the energy balance between the Van der Waals forces and the electrostatic forces, as it possible to see in Figure 3.1.4.
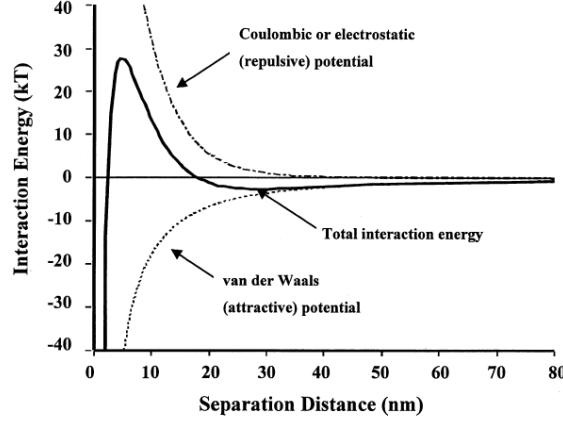
Figure 3.4. Interaction energies in colloidal suspensions [35].

Oil-based colloid In the case of apolar medium, stabilized suspensions are created by absorbing surfactants on the particle surface. These active materials have a dual purpose, since they balance the solubility and the reactivity of the particle with the solvent. For example, in the case of kerosene-based ferrofluid, the magnetite particles are covered by the oleic acid, that reduces the surface tension between the particles and the solvent. Steric stabilization is the only way to obtain stable colloidal suspension in apolar solvents, because the barrier against agglomeration gives hydrophobic properties to the polar nanoparticles.

For spherical nanoparticles, if we consider long chained molecules, the steric energy can be defined as [14]:

$$E_{Steric} = \frac{k_B T \pi D^2 \zeta}{2} \left[2 - \frac{x+2}{t} \ln \left(\frac{1+t}{1+x/2} \right) - \frac{x}{t} \right] \tag{3.16}$$

where ζ is the surface density of the surfactants molecules and t is the normalized thickness of the surfactant with s the thickness of the surfactant:

$$t = \frac{2s}{D}$$

As in the previous case, the cumulative action of the steric repulsion and the Van der Waals forces generates a minimum in the potential energy. However, the surfactants in this case provides an energy barrier that do not permit to the particle to be in contact and therefore this avoids the coagulation due to attractive forces. Furthermore, if the surfactant matches the dielectric properties of the carrier liquid, it reduces the Hamaker constant A to zero and this guarantees the stability in the colloidal system.

55

3.2 Ferrofluid

In nature, it is not possible to find a fluid that becomes strongly magnetized in presence of an external magnetic field. This is mainly due to the fact that liquid ferromagnetic materials are present in natural state only at temperatures above their Curie's temperature. However, exploiting the properties of colloids, in 1963 Steve Papell in NASA's laboratories developed a process to synthesize a superparamagnetic fluid, named ferrofluid. According to the definition of Rosensweig [17], ferrofluids are a colloidal solution composed by nanoparticles of ferromagnetic material suspended in a carrier liquid (organic solvent, hydrocarbon or water). The particles are coated with a surfactant (oleic acid for oil-based, anionic or cationic dispersant for water-based), that prevents agglomeration.
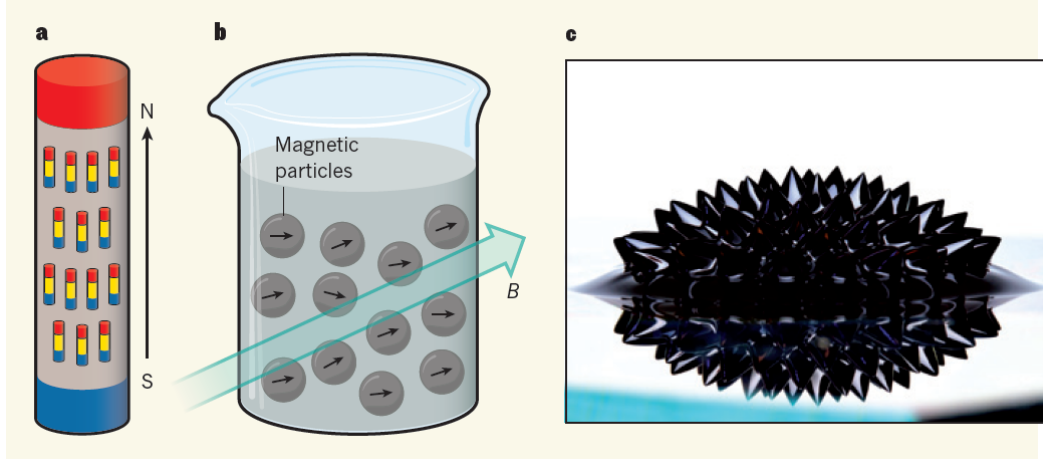
Figure 3.5. Bar magnets and ferrofluids. **a**, Ferromagnetic iron, the magnetic moments of iron atoms maintain their mutual north-south magnetization in absence of a magnetic field. **b**, Ferrofluids, suspensions of nanometric ferromagnetic particles, respond strongly to an applied magnetic field (superparamagnetic behaviour). **c**, Photograph of a ferrofluid sujected to an external magnetic field with its peculiar spikes [38].

The fascination of ferrofluids arises from the fact that their flow and properties can be significantly altered by the influence of moderate magnetic fields [39]. The possibility to control a fluid using an external magnetic field opens a wide spectrum of possibilities in different fields of applications, from passive cooling systems in low gravity environments to biomedical applications.
Moreover, it is possible to recover and harvest electrical energy from the motion of the magnetic fluid, exploiting its magnetization and demagnetization properties.

3.2.1 Fe_3O_4 ferrofluid

Nowadays, there exist a wide range of materials that can be used as ferrofluids. The choice of the material and of the carrier liquid is strictly dependent on the field of application, the physical properties of the colloidal solution and the price on the market.

Magnetite-based ferrofluid are currently used for different applications, mainly because the synthesis technology was patented in the 60's and so, the relative price is very competitive in the industrial market.

Nanocrystalline magnetic iron oxide particles for MFs are usually prepared by wet-chemical precipitation from aqueous iron salt solution by means of alkaline solution like KOH or NH_4OH [39], knowing that:

$$Fe^{2+} + 2Fe^{3+} + 8OH^- \rightarrow Fe_3O_4 + 4H_2O \tag{3.17}$$

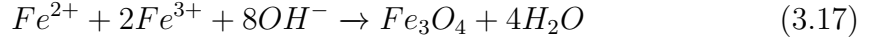This precipitation method permits to synthesize particles with a mean diameter of 10 to 30 nm, according to precipitation parameters. Usually, a single-cycle synthesis provides particles with a broad range of distribution. However, the most common technique to avoid this effect consist in a multi-phase synthesis: a 1 M of $NaHCO_3$ solution is slowly added to $FeCl_2/FeCl_3$ (ratio 1:1) under permanent stirring up to pH = 7. Then, a new Fe^{2+}/Fe^{3+} solution is added as in the first cycle, and the precipitation is carried out again. This procedures can be repeated three of four times. Finally, the solution is boiled for 10 minutes, then washed and dried [39].

To characterize the solution, there is an interesting technique that permits to define the diameter distribution of the synthesized particles in a easy way. If the solution is highly diluted, the magnetic interparticle interaction can be neglected [39]. This means that the magnetization of the solution can be described using the Langevin relation Eq.2.29. Applying a small magnetic field, the Langevin relation can be linearized using a first order Taylor expansion and considering the diameter dependence on this relation we obtain that:

$$\chi_i = \frac{1}{3}\Phi M_d \frac{\mu_0 M V}{k_B T}$$

Measuring the magnetization of the solution it is possible to have an indication of the mean diameter of the particles. But, if we suppose that the diameter distribution can be fitted using a log-normal size distribution, we obtain that:

$$M = M_s \int_0^\infty L(\beta) f(y) dy \qquad f(y) = \frac{1}{y\sigma\sqrt{2\pi}} \exp\left[\frac{-(\ln y)^2}{2\sigma}\right] \tag{3.18}$$

where y is the normalized particle diameter, f(y) representing the mentioned log-normal size distribution in the form, σ the width of the distribution of a measured magnetization curve and $L(\beta)$ is the Langevin equation Eq.2.30. So, the measure of the magnetization response of the solution in an homogeneous sample can give a quantitative indication of the distribution of the particles' diameter.

3.2.2 Applications

The possibility to control the flow properties of a liquid using magnetic systems has led to the development of a wide range of possible applications for ferrofluids, in different research fields.

In the mechanical field, the most famous application is the sealing of a rotating shaft. A rotating shaft is composed by a material with high permeability surrounded by a permanent magnet. The gap between the two materials is in the order of few millimeters, so the magnetic field intensity in this region will reach 1 T of magnitude. If a ferrofluid is placed into the gap, the magnetic forces acting on the fluid can hold the fluid in this position even if a pressure difference is applied to both sides of this liquid seal. This can be easily explained using the modified magnetic Bernoulli equation [39].

Another important aspect that can be exploited is the variation of viscosity in the fluid due to the application of an external magnetic field. Clutches, brakes and dampers have been designed introducing a magnetic controllable element through integrated circuits in order to modify locally the damping properties of a system. Also, in the case of brakes, the ferrofluid can be used for its passive properties for thermal exchange. In particular, the magnetic fluid exhibits an increase of thermal conductance when a magnetic field is applied [40], leading to a controllable change of thermal properties of the system. Nowadays, the ferrofluid is mainly employed in the loudspeaker systems as heat transfer medium, reducing the increase of temperature in the case of ohmic heat transfer and so, increasing the maximum acoustic power of the speaker. Another important application is the heat trasfer using magnetoconvection in the case of low-gravity condition. A more detailed analysis about this phenomenon is explained in Sec.2.3.2.

The third important field that should be mentioned is the use of ferrolfuid in medical applications. In particular, in the theranostic field the magnetic nanoparticles are used for the cancer treatment by hyperthermia: the surfactant layer is functionalized with drugs or biological markers and afterwards the fluid is injected in the patient. Exploiting the enhanced permeation and retention (EPR) effect or the right functionalization of the carrier surface, the nanoparticles will attach on the cancer site. Finally, applying locally an AC-field, the nanoparticles will dissipate this energy through a local increase of temperature, which will damage the tumor tissue [39].

3.2.3 Physical properties

Viscosity in Ferrofluid: Concentration dependence and Magnetoviscous effects

The viscosity of a fluid represents the resistence to deformation at a given rate of stress. From a mathematical point of view, considering a cartesian system of coordinates, the viscosity can be defined as:

$$\tau_{ij} = \sum_i \sum_k \eta_{ijkl} \frac{\partial v_k}{\partial r_l}$$

where η_{ijkl} is the viscosity tensor (constant for Newtonian fluid - isotropic properties), τ_{ij} is the viscous stress tensor and $\partial v_k/\partial r_l$ the strain rate tensor.
Generally speaking, the viscosity of a suspension will vary from that of the carrier liquid due to the presence of the suspended particles. In the case of non interacting particles, there is a linear relation developed by Einstein that states [14]:

$$\eta_0 = \eta_c \left(1 + \frac{5}{2}\Phi_s \right) \tag{3.19}$$

where η_0 is the viscosity of the suspension in absence of a magnetic field, η_c the viscosity of the carrier liquid and Φ_s the modified volume concentration of particles, including the geometrical dimensions of the surfactant:

$$\Phi_s = \Phi \left(\frac{(d+2s)}{d} \right)^3 \tag{3.20}$$

where d is the particle diameter and s is the surfactanct length. This relation is valid only in the case of highly diluted solutions, because increasing the concentration of the suspended phase the particles tend to interact each other, generating complex chained structures [14].
It is possible to take into account this effect considering that the viscosity should diverge for a particular critical volume fraction Φ_c. So including a quadratic term in the previous linear equation, we obtain that:

$$\eta_0 = \eta_c \left[1 - \frac{5}{2}\Phi_s + \left(\frac{5}{2}\Phi_c - 1 \right) \left(\frac{\Phi_s}{\Phi_c} \right)^2 \right]^{-1} \tag{3.21}$$

Usually $\Phi_c = 0.74$ is assumed when the Eq.3.21 is used for comparison with experiments.
Volume fractions below $\Phi = 0.11$ are well described by the previous formula, but increasing the concentration the particle-particle interaction plays a dominating role in this aspect.
Another common way to increase this interparticle interaction is to apply a magnetic field: in this case we can talk about magnetoviscous effects.
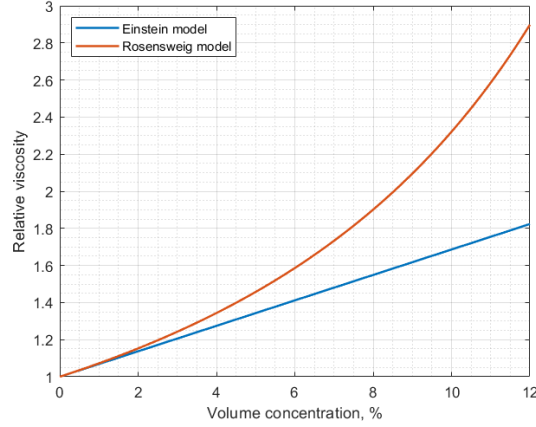
Figure 3.6.   Difference between Einstein and Rosensweig model for relative viscosity in EFH3 ferrofluid. The kerosene dynamic viscosity is $\eta_c = 1.92 \times 10^{-3}$.

An interesting model provided by Odenbach et al.[14] describes this phenomenon as the variation of the local concentration of bidisperse systems, containing a small fraction of large particles that forming chains in presence of an external magnetic field and a large amount of particles with weak interparticle interaction.

Starting from the continuity equation, it is possible to define the temporal changes of the concentration distribution of magnetic particles as:

$$\frac{\partial c}{\partial t} + \nabla \cdot \mathbf{J} = 0 \tag{3.22}$$

where c is the particle concentration, $\mathbf{J}$ is the total flux of particles, composed by a diffusion component (Fick's law) $\mathbf{J}_d$ and a drift component $\mathbf{J}_f$, driven by external forces:

$$\mathbf{J} = \mathbf{J}_d + \mathbf{J}_f = -D\nabla c + \mathbf{v}_p\, c \tag{3.23}$$

where D is the diffusion coefficient and $\mathbf{v}_p$ is the particles velocity. In a simple model, it is possible to assume that the diffusion coefficient is independent from the concentration, described by the Nernst-Einstein relation, and the drift velocity is mainly induced by the magnetic force:

$$\frac{\partial c}{\partial t} = \frac{1}{6\pi\eta r}\left[k_B T(\nabla^2 c) - \nabla(c\,\mu_0 V_{NP} M_d \nabla H)\right] \tag{3.24}$$

where r is the Stokes' particle radius and η is again the viscosity.

In this case, considering the steady-state condition and a fluid composed by particles with distributed-diameter, it is possible to state that particles which are smaller than 10 nm hardly react on the field gradient, while the concentration of the fraction of bigger particles remains fixed in the region of high magnetic field.

According to this behaviour, it is possible to describe in a better way the magnetoviscous effect. First of all, in zero magnetic field, the dependence between stress and shear rate in both fractions should be linear (with particle concentration below 11%). That means the fluid should behave Newtonian, since no field induced interparticle interactions leading to chains or clusters are present. So, in this case the ferrofluid behaves like a normal suspension of non-magnetic particles.

However, applying magnetic fields, the fluid with a large concentration of bigger particles has a stronger magnetoviscous effect with with respect to the original fluid, due to the particle/particle interactions. This implies that the relation between the shear and the stress is not anymore linear. Vice versa, the part of the fluid that is defined "far" from the magnet source presents a Newtonian behaviour.

Concentration dependence of magnetic permeability in ferrofluid

Ivanov A. et al. [41] [42] proposed a mathematical model that permits to define the magnetic susceptibility of with ferrocolloids as function of the volume concentration of paramagnetic particles.With respect to the classical Langevin relation, they consider the magnetization as the combination of the external field H_0 and of the collective magnetic field produced by other particles. This theory introduces also a demagnetization factor, due to the change of shape of the particles when they are subjected to an external magnetic field.

As first assumption, they suppose that all the magnetite particles equal in volume V_d, the internal magnetic field inside the droplet is uniform and the fluid is homogeneous. To describe the magnetic parameters of a ferrofluid, it is possible to use the first order modified mean-field model, that takes into account a linearization of the inter-particle interaction. In this case, the ferrofluid magnetization M is given by:

$$M(H) = M_L(H_e) \qquad H_e = H + \frac{4\pi}{3} M_s L \left(\frac{mB}{k_B T} \right) \tag{3.25}$$

where $L(x)$ is the Langevin equation, $M_L(x)$ is the Langevin relation and M_s is the saturation magnetization.

The relative magnetic permeability μ_e could be defined as:

$$\mu_r = 1 + \Phi \frac{M_d(H_d)}{H_0} = 1 + \chi \tag{3.26}$$

where H_0 is the intensity of the external magnetic. This definition takes into account that the magnetic permeability of the carrier liquid is equal to the unity. If we consider the Langevin relation Eq.2.31 (non-iteracting model) for spherical particles, the relative magnetic permeability can be written as:

$$\mu_r = 1 + \Phi M_d \frac{\mu_0 m}{3k_B T} = 1 + \Phi \chi_i \tag{3.27}$$

where χ_i is defined as the intial magnetic susceptibility.

If we want to consider the variation of eccentricity of the particle, due to the action of an external magnetic field, we have to define a demagnetization factor $n_z(e)$ as function of the ellipsoid eccentricity e:

$$n_z(e) = \frac{1 - e^2}{2e^3} \left[\ln \left(\frac{1 + e}{1 - e} \right) - 2e \right] \tag{3.28}$$

We are assuming that the shape of the particle is defined and unperturbed, i.e. we are considering a magnetostatic case. It is important to note that according to the intensity of the applied magnetic field, the droplets can change their shape, passing from a spherical shape to an ellipsoidal one. This change of shape causes a reduction of the droplet magnetization, that is taken into account by the demagnetization factor.

In the weak-field limit, when the linear magnetization law $M_d = \chi_i H_d$ holds true, it is possible to define the initial magnetic permeability of the ferrofluid emulsion as:

$$\mu_r = 1 + \frac{\chi_i \Phi}{1 + \chi_i n_z(e)(1 - \Phi)} \tag{3.29}$$

Finally, if the particle shape remains spherical, we have that the eccentricity of the particle is equal to zero. Therefore, we obtain that:

$$\lim_{e \to 0} n_z(e) = \frac{1}{3} \qquad \mu_r = 1 + \frac{\chi_i \Phi}{1 + \frac{1}{3}\chi_i(1 - \Phi)} \tag{3.30}$$

This formulation is valid since we remain in the weak field limit and the particles are considered spherical. However, in order to have a very accurate quantitative model, we must take into account the demagnetization factor according with the eccentricity of the particles and considering also the inter-droplet aggregation. This latter is more evident as long as the concentration of particles and/or the applied magnetic field increases.

In particular, Dikansky Y. et al. [43] proposed an experimental analysis to evaluate the maximum concentration of magnetite particles dispersed in kerosene solvent to confirm the validity of the classical dipolar model. Studying the dependence of relaxation time with respect to the temperature, they found that for concentrations below 8% in volume the fluid follows the behaviour expressed by the Curie's law. However, for higher concentration there is a violation of homogeneity of the samples, due to the formation of aggregates. So, the impact of the local fields generated by the particle's neighbourhood, give a contribution for the orientation of the particle moment along the applied field direction.
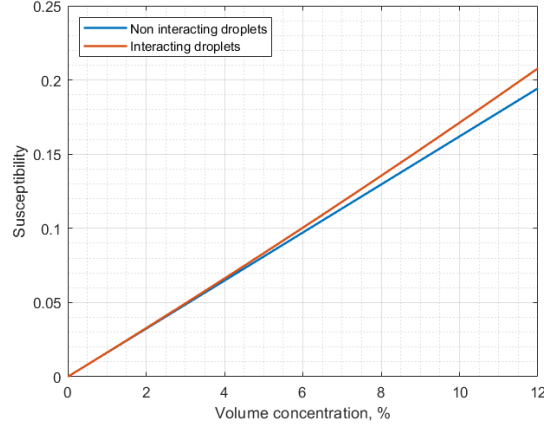
Figure 3.7. Difference between interacting and non-interacting model for relative magnetic permeability of ferrofluid EFH3. The initial magnetic susceptibility χ_i = 3.53 from the manufacturer datasheet at 25° C.

Concentration dependence of thermodynamic parameters in ferrofluid

The presence of ferromagnetic particles in a carrier fluid changes also the thermodynamic behaviour of the fluid. From a preliminary analysis, it is possible to model the fluid as single-phase mixture in thermal equilibrium. According with this statement, the specific heat of a generic colloidal suspension C_P, with concentration of solid particles Φ can be modeled as:

$$C_P = \frac{(1 - \Phi)\rho_f C_{pf} + \Phi \rho_p C_{pp}}{\rho} \qquad \rho = (1 - \Phi)\rho_f + \Phi \rho_p \qquad (3.31)$$

where ρ_f is the density of the carrier fluid, C_{pf} is the specific heat of the fluid, ρ_p the density of the particles and C_{pp} the specific heat of the particle. Using the same approach, the thermal conductivity of a colloidal mixture can be defined as:

$$\kappa_F = \kappa_c \frac{2\kappa_c + \kappa_d - 2\Phi(\kappa_c - \kappa_d)}{2\kappa_c + \kappa_d + 2\Phi(\kappa_c - \kappa_d)} \qquad (3.32)$$

where κ_F is the thermal conductivity of the mixture, κ_c of the continuous phase and κ_d of the particles [44]. However, a more complex model can take into account the effects of the Brownian motion and the magnetic interaction between particles. In particular, the action of an external magnetic field can define inside the mixture short-chained structures,which changes the distribution pattern of the particles from homogeneous dispersion medium to a non-uniform aggregated particles[2].

---

[2]If the reader is interested in the variation of the thermodynamic variables in presence of an external magnetic field can consult the document [40].

Chapter 4

Experimental Setup

The CERES System consists in a complex setup, where it is possible to recover electric energy from the thermally driven motion of a colloidal solution, that generates different flow patterns. The velocity profile is mainly characterized by the typical flow associated to natural convection (Rayleigh–Bénard convection and Vertical convection). However, the presence of a superparamagnetic fluid implies that it is possible to modify the motion pattern applying local magnetic fields using permanent magnets, inducing the thermomagnetic advection.

So, the idea behind the project is to induce a periodic motion along the toroidal axis of the reactor, exploiting the thermomagnetic properties of the fluid. The prototyping of such device is very complex from different points of view, since the motion generation part and the recovery system of the device are not linearly independent. In fact, in order to define a stable and unperturbed fluid motion with a stable electric output power, it is necessary to take into account: the geometry of the system (toroidal), the aspect ratio of the chamber, the material of the tank and the colloidal solution, the heat exchange between the waste heat and the solution, the choice of the magnets (magnitude and position), the correct installation of the device (vertical or horizontal alignment to the heat source) with respect to the application (industrial, automotive or wearable). Therefore, the best way to proceed during the prototyping process is the "divide et impera".

In this thesis project, we decided to decouple the motion generation part from the recovery part of the system. In this way, it was possible to do a correct electric characterization of the open-circuit voltage and short-circuit current generated by the magnetization and demagnetization of a ferrofluid, when it is subject to the action of a permanent magnet. So, the experimental setup was defined in a simple way: the colloidal solution is pumped in a cylindrical pipe through a peristaltic pump; the extraction region was defined at the centre of the pipe, in order to reduce the turbolent effects associated to the variation of the section of the pipe. In this way, it was also possible to use the same setup in order to show the physical feasibility of the triboelectric effect, induced by the fluid friction between a
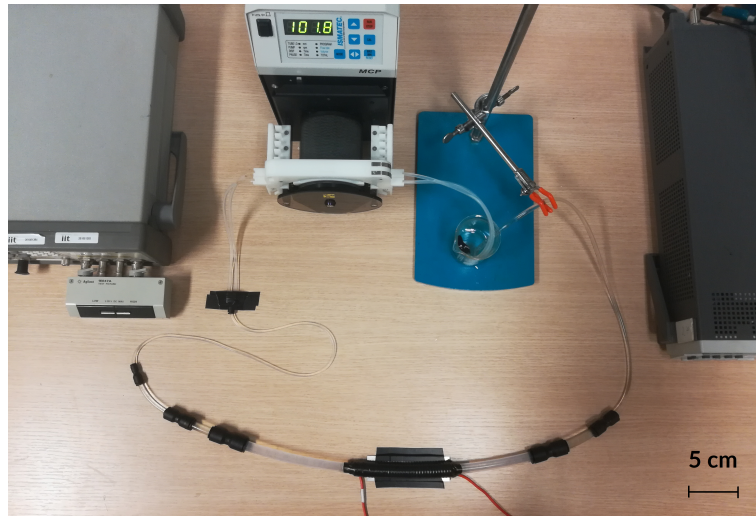
Figure 4.1.   Experimental setup for inductive and capacitive characterization. At the centre it is possible to observe the peristaltic pump for the motion generation, that is directly connected to test solution contained in a becher; the pump was linked to a series of pipes with different diameters and conneceted together by hydraulic adapters; the main pipe was made in FEP (internal d = 10 mm, external D = 12 mm) and the extraction electrode was placed at the center of this pipe. In the case of inductive characterization of ferrofluid, a permanent magnet array was placed behind the solenoid.
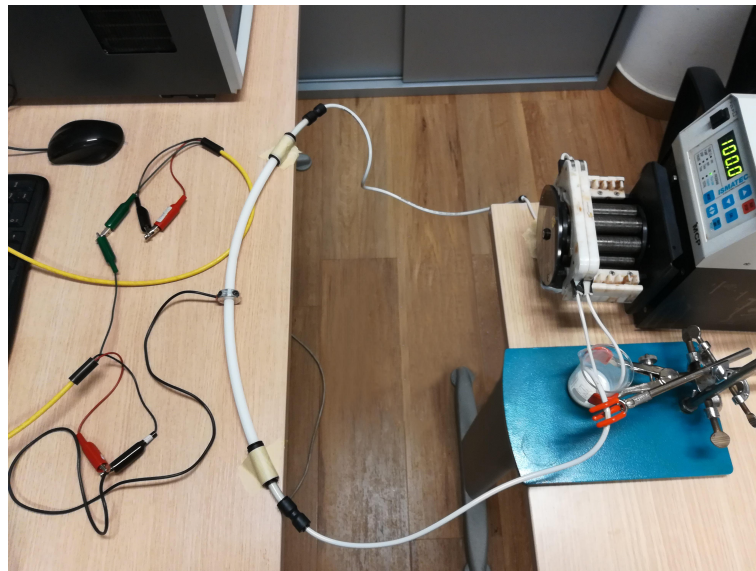

Figure 4.2.   Example of capacitive experimental setup, with an aluminuim ring as primary electrode (Single-Electrode Mode).

water-based colloidal solution (titania powder) and the FEP pipe. The choice of the triboelectric effect was done considering the complementary recovery behaviour with respect to an induction recovery system: usually the triboelectric effect generates high voltage and low current, while the induction system has low voltages and high currents. Finally, a permanent magnet-solenoidal coil was used for the ferrofluid characterization, while an aluminuim ring was used for the capacitive characterization of the triboelectric solution. The electrical characterization consisted in a open-circuit voltage and short-circuit current measurements for both effects (triboelectricity analysed in Single-Electrode Mode) and for the inductive characterization we did also an impedence analysis.

4.1   Motion generation and Pipe system

A peristaltic pump is defined as a positive displacement pump, where a fluid contained within a flexible tube (silicone in our case) is compressed in a periodic way, using rollers systems. As the rotor turns, the part of the tube under compression is pinched closed, forcing the fluid to move through the tube in the rotational direction.
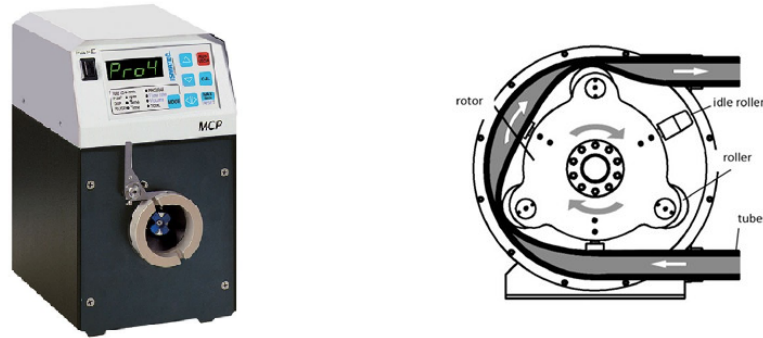

Figure 4.3.   Ismatec MCP peristaltic pump (left). Schematic of the working principle of a peristaltic pump (right).

The pressure pattern is defined as peristalsis, and so it defines a pulsed flux of the fluid, that changes shape and velocity according with the rotational speed of the rotor. The pump can generate a flow rate that changes according to the internal diameter of the compressed pipe. The Ismatec MCP provides a rotor system that allows only pipes with a maximum internal diameter of d = 3.2 mm. This permits to generate at the maximum rotational speed a flow rate of 100 mL/min for each channel, up to 8 channels.

The pipe system consisted in a series of different tubes that could be easily interfaced with the peristaltic pump. In particular, we used a silicone pipe (d = 3.2 mm - D = 4 mm) that was perfectly adaptable with the rotor system of the peristaltic pump; after that, we changed the pipe diameter with a series of adapters. The test pipe was made in FEP with an internal diameter of d = 10 mm and an external diameter of D = 12 mm. The choice of the material was made for its triboelectric properties and for its chemical compatibility with the oil-based ferrolfuid. Fluorinated ethylene propylene is defined as negative element in the triboelectric series, due to its fluorinated groups in the polymeric structure. Having the water a tendency to charge positively in presence of very electronegative elements, this makes FEP the perfect candidate for the study of triboelectric effects.

The sizing of the pipe was made doing some assumptions in the dynamics of the fluid. First of all, we consider cylindrical pipes, where the modes of propagation are well-established in literature, due to its simple dynamics. So, the sizing of the pipe was mainly done choosing the diameter of the pipe and analysing the economic feasibility of the material and the availability on the market.
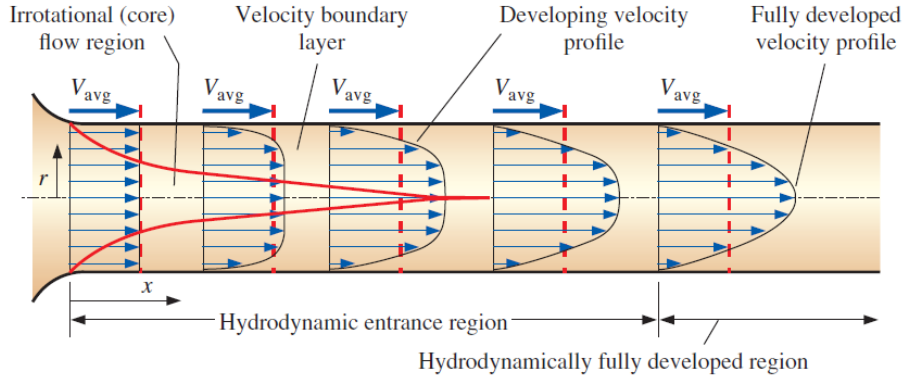

Figure 4.4.   Example of the laminar flow in a cylindrical pipe.

On the one hand, we wanted to have a laminar flow in the case of ferrofluid applications, because in this case it is possible to have a priori an idea of the velocity profile (Poiseuille flow). This is an important consideration to do, since laminar flow along a specific direction gives an important contribution to the electromotive force generated by the motion of the ferrolfuid (Eq.2.76). However, in this phase of prototyping we didn't take into account the magnetoviscous effects, the turbolence effects introduced by the change of dimensions of the pipes due to the adapters and the non-continuous flow generated by the peristaltic pump.

On the other hand, using the same assumptions, we wanted to introduce a turbolence component in the case of water based solutions. In this case, we supposed to

have a more evident triboelectric behaviour associated to the fluid friction on the pipe walls.

So, knowing that the peristaltic pump can guarantee a fixed value of flow rate, it is consequently possible to define the mean velocity in the pipe:

$$Q = \mathbf{v} \cdot \mathbf{A} = \langle v \rangle \frac{D^2}{4} \pi$$

where $\langle v \rangle$ is the mean velocity of the fluid parallel to the normal unit vector of the surface A, which is defined as $D^2\,\pi/4$ in the case of cylindrical pipe. The flow analysis was simply done considering the Reynolds number associated to the system:

$$Re = \frac{\rho d v}{\eta}$$

where ρ is the density of the fluid, d the internal diameter of the pipe, v the mean velocity of the fluid and η the dynamic viscosity. It is a dimentionless number that represents the ratio between the intertial forces in the fluid and the viscous forces and it gives an indication on the transition between the laminar flow to the turbolent flow. Generally, in literature it is reported that if $Re < 2{,}000$ the flow is laminar and if $Re > 4{,}000$ the flow is turbolent.
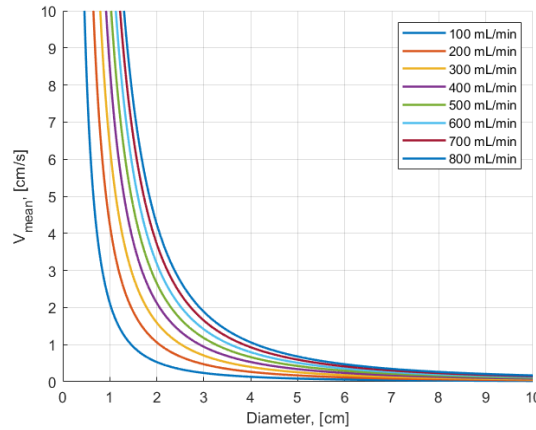

Figure 4.5.   Values of mean velocity that changes according to the flow rate and the diameter of the pipe.

According to these definitions, we first defined a range of velocity magnitude that could be comparable to the velocities generated by a natural convection process. We fixed thus the maximum value to $v = 5$ cm/s. Knowing that the peristaltic pump has eight channels with a maximum flow rate of 100 mL/min per channel, we defined how many sources we needed in order to reach this value of velocity with a

fixed diameter.

After that, we defined the Reynolds number associated to the different solutions, considering the physical parameters of the ferrolfuid ($\Phi = 0.08$) and the pure water.
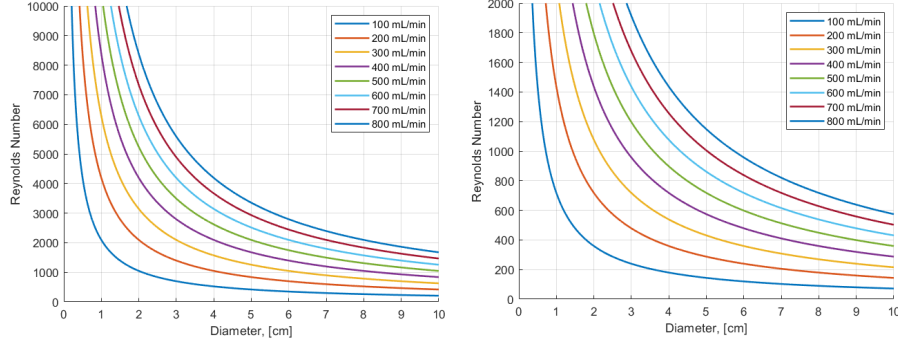

Figure 4.6. Reynolds number associated to pure water (left side) and to a EFH3 ferrolfuid solution at $\phi = 0.08$ (right side), that changes according to he flow rate and the diameter of the pipe.

Finally, we found that the best solution was to use a FEP pipe with a 10 mm of internal diameter with two channels of the peristaltic pump.

4.2   AlNiCo Magnets

AlNiCo (aluminuim-Nickel-Cobalt) is a family of iron alloys that presents a ferromagnetic behaviour and are mainly used for the realization of permanent magnets. The composition of AlNiCo alloys is typically 8–12% Al, 15–26% Ni, 5–24% Co, up to 6% Cu, up to 1% Ti, and the balance is Fe. The choice of this material is mainly related to its cost and to its stable magnetic properties at temperatures that are compatible with the low enthalpy sources (maximum allowable 150 °C).

We use AlNiCo permanent magnets in order to induce magnetization in the ferrofluid solution. The magnetic profile of the magnets are very important for the characterization of the system, since the mutual action of the velocity profile and the gradient of magnetization along the extraction coil determines the electromotive force that can be extracted in the system (Eq.2.76).

To understand better which is the profile generated by an array of magnets, we defined the magnetic potential generated by an horizontal (with respect to the reference plane) magnetization source. The model of the magnet was done considering a magnetic dipole approximation, in which the magnetic potential Ψ can be defined as:

$$\Psi = \frac{\mathbf{m} \cdot \mathbf{r}}{4\pi r^3} \qquad \mathbf{H} = -\nabla\Psi$$
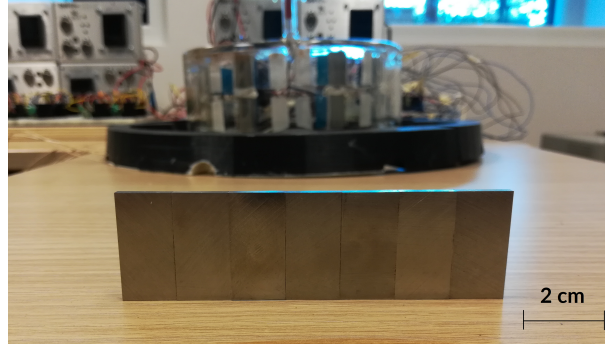
Figure 4.7.   Example of AlNiCo magnetic array used in the experimental setup.

Supposing that the magnet is located above the pipe and the edges are represented in Fig.4.2 as the yellow and blue spot, we obtain:
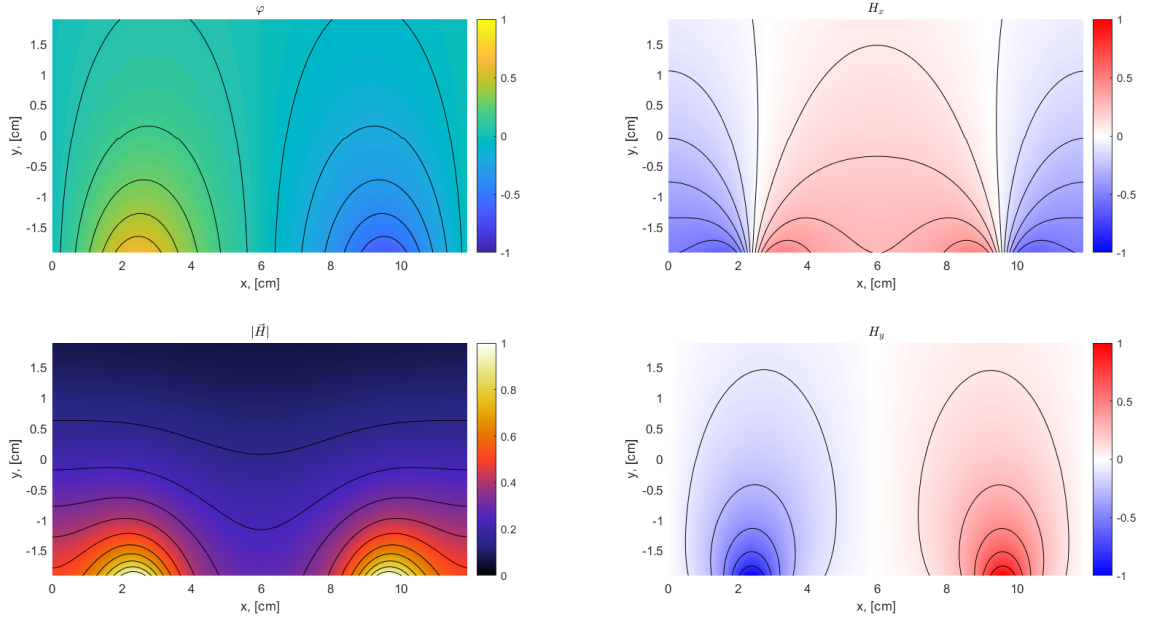

Figure 4.8.   Numerical evaluation of the magnetic field generated by an array of permanent magnets with horizontal magnetization.

To understand the effectiveness of this simple model, we characterized the x-component of the magnets using a Gaussmeter - Hirst Magnetics GM08. This instrument exploits the Hall effect in order to measure the magnetic strength of a generic source. After an automatic calibration of the instrument, we obtained the following results. In particular, the x-component of the magnetic field is evaluated in the xy plane in contact to the permanent magnets.
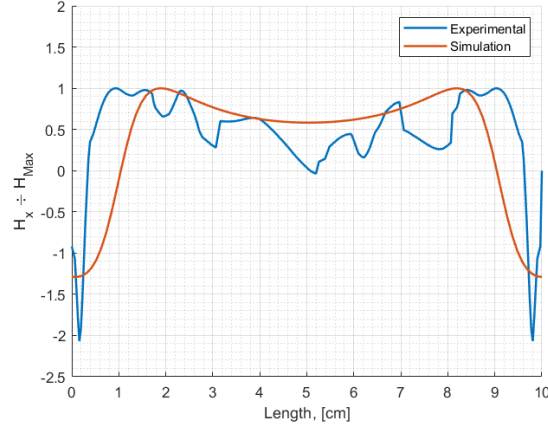
Figure 4.9.   Comparison between the numerical and experimental results of the H_x field generated by a permanent magnet array.

The numerical and experimental results are quite comparable. In this case, we represented only normalised results, because the physical properties of the permanent magnets where not provided by the constructor. The variation of the field in the experimental results can be mainly associated to the fact that the permanent magnet is not a single body, so the magnetic field lines can be closed at the interface between the single magnets. However, it is possible to observe that there is a minimum in the centre of the array, and on the other two sides there is with respectively a positive and negative slope. Again, considering the Eq.2.76, the gradient of magnetization is an important value for the evaluation of the electromotive force. So, we defined as the best solution to impose two different arrays of magnets at the edges of the extraction system (solenoid) and impose the polarity as S-N N-S. In this way, inside the coil region, there will be the same slope of the magnetic field, and so the same gradient value.

4.3   Colloidal solution

4.3.1   Ferrofluid - Ferrotec EFH3

We used an EFH3 ferrofluid, purchased by Ferrotec. EFH3 ferrofluid is magnetite-based, dispersed in light hydrocarbon carrier. The steric stabilization was made using oleic acid. It is sold at concentration of 11.8% an its appearance is black-brown, with a mean diameter of 10 nm and a surfactant length of 2 nm.

	EFH3
Saturation Magnetization (M_s)	51 kA/m
Initial Magnetic Susceptibility (χ_i)	3.52
Pyromagnetic coefficient (K)	30 A/m °C
Viscosity @27 °C	12 mPa s
Density @25 °C	1.42×10^3 kg/m^3
Pour Point	-94 °C
Flash Point	92 °C
Volumetric Concentration	11.8 %

Table 4.1.   Physical parameters of Ferrotech EFH3.

4.3.2   Titania paste

For the triboelectric effect, we dispersed titanium dioxide TiO_2 (purchased by Degussa) in pure water. We used a 30 nm titania powder, with a compositon of 40% rutile and 60% anatase. The colloidal solution was made only dispersing the powder in a ultrasonic bath for 30 minutes.

Figure 4.10.   Water based colloidal solution with TiO_2 dispersed (left sample with volume concentration of 4% and right sample with 2%.)

4.4 Extraction and characterization systems

The extraction system consist of a solenoid coil for the inductive characterization (ferrofluid) and an aluminium electrode, that is anchored around the FEP pipe, for the single electrode mode characterization.

The solenoid is realized by rolling up a low resistance copper cable around the tube. In this case, the solenoid presents 40 windings around the tube, with a diameter of D = 12 mm, a cable thickness of t = 2.5 mm, in a length of L = 100 mm. This system will be the element that permits to detect the induced electromotive force, since there will be a variation of the relative magnetic permeability due to the flowing of the ferrofluid in the pipe. Note that it can be possible only if there is a variation of magnetization in the fluid in the region of extraction, i.e inside the solenoid.
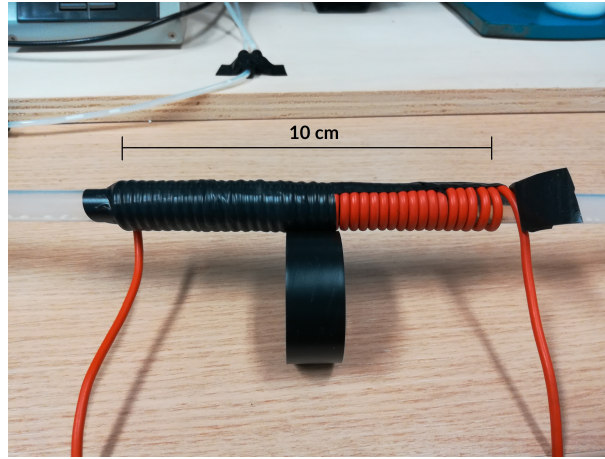

Figure 4.11.   Installation of the solenoid around the FEP pipe.

For the inductive characterization, it was possible to do an open-circuit voltage measurement using SourceMeter - Keithley 2635A, a measure of short-circuit voltage with Semiconductor characterization system Keithley 4200-SCS, coupled with a low-noise amplifier Keithley 4225-RPM and an impedence analysis (Resistence R and Reactance X) with an impedencemeter Agilent E4980A. For the VI characterization we used two different instruments, because of the sensibility on the current or voltage measurement. In particular, the characterization system Keithley 4200-SCS has a current resolution of 10 aA if associated with the optional amplifier (Keithley 4225-RPM).

For the capacitive characterization, we used an aluminuim ring electrode as a primary electrode. The choice of aluminuim was made considering the triboelectric coupling with the FEP material, having Al the tendency to accumulate positive charges on its surface. The reference electrode is chosen as the same ground of

the measuremet instrument, in order to guarantee the repeatability of the measure. The Al ring is a screw clamp, characterized by a 12 mm of internal diameter, 28 mm of external diameter and a length of 11 mm. In this case it was not possible to do an impedence analysis, since we are dealing with a single electrode device.

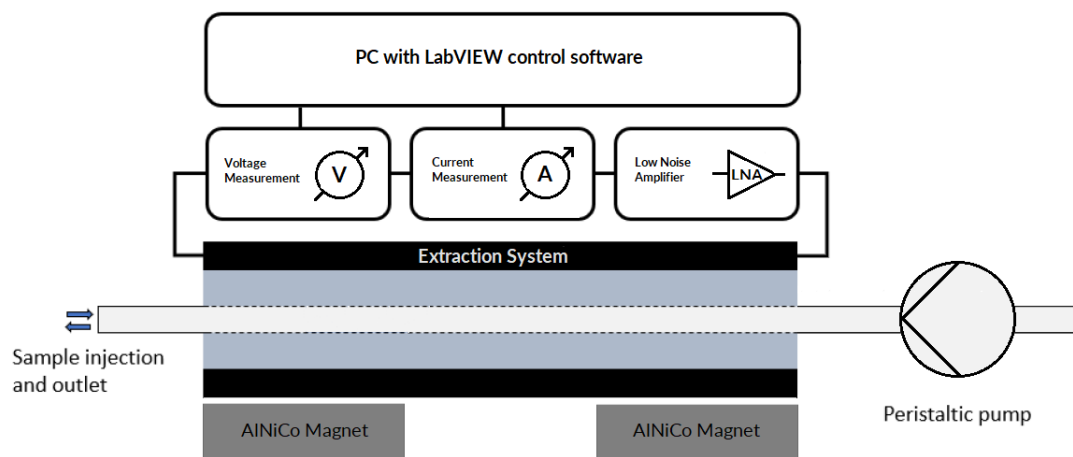Figure 4.12. aluminuim ring used for the capactive characterization in Single Electrode Mode.

Figure 4.13. Sketch of the extraction and characterization system.

75

Chapter 5

Data Analysis

In this Chapter, the data collected from the measurement will be plotted in graphs and consequently analyzed. The procedure of acquisition is the same for the capacitive and inductive electrodes: it is possible to observe which is the electrical behaviour of the device, varying the mean velocity inside the pipe, using the peristaltic pump. In particular, we choose a set of velocities, ranging from 1 cm/s to 5 cm/s. After the first collection of the raw data it was possible to select a subset, neglecting the transient of the measurement, due to the capacitive and inductive coupling between the device and the characterization system. Finally, the selected data are filtered using a first order Savitzky–Golay filter (Moving-Average filter). All the data are compared with respect to their relative offset diagram, that is evaluated considering the idle condition of the fluid (pump-off reference). Consequently, the data are plotted in a Voltage-Velocity and Current-Velocity diagram.

5.1   Inductive characterization of Ferrofluid

The procedure to collect data from the inductive characterization consists in the evaluation of the electromotive force generated in the central region of the FEP pipe, where a static magnetic field is applied by using two different array of Al-NiCo magnets. In this way it was possible to induce a more evident gradient of magnetization in the ferrofluid, along the direction of the flow (see Chapter 4). Using the Gaussmeter, it was possible to define the values of the magnetic field strength, that span linearly from 30 kA/m to 3 kA/m.
We defined the electric behaviour for three samples, changing the concentration of the ferrofluid from 2% to 6%. In this way, it was possible to directly observe how the recovery mechanism works and how the influence of the magnets affects the motion generation in the fluid.
Considering the voltage measurement, it is possible to observe the typical time behaviour of a RLC circuit (Resistor-Inductor-Capacitor), in which the inductive

component is defined by the solenoidal electrode and the resistive-capacitive part is given by the measurement instrumentation. In particular, the step response of voltage and current shows a damped behaviour and so, the system reaches the stability after a time transient.

In order to measure V_{OC} and I_{SC} at the equilibrium, first of all we choose a data subset associated to the last part of the measurement. After that, we applied a moving average filter (first-order polynomial Savitzky-Golay filter), with a fixed filtering window of 51 samples. The choice of this filtering window was related to the minimization of the error band, due to the natural damping of the RLC circuit. It is important to note that for the voltage measurement we were able to acquire 3 samples for second, while for the current measurement it was possible to take 15 samples for second. The limitation was given by the instrumentation.
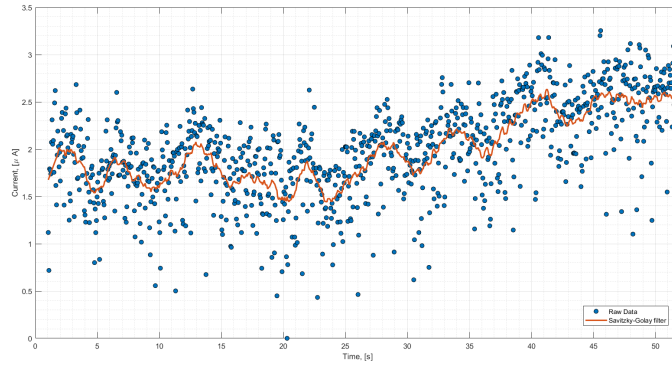

Figure 5.1. Time-Current measurement. Comparison between the raw data and the filtered one (S-G polynomial order = 1, filtering window = 51 points).
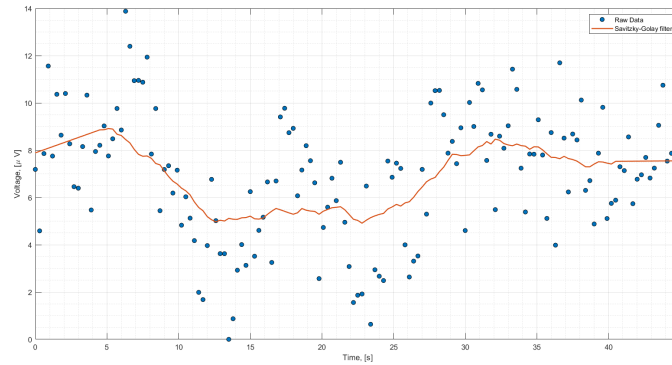

Figure 5.2. Time-Voltage measurement. Comparison between the raw data and the filtered one (S-G polynomial order = 1, filtering window = 51 points).

78

5.1.1 Volume concentration 2%

For what concerns the inductive characterization, first of all we did an impedance analysis. This is an important technique for the analysis of the equivalent circuit associated to the system. In order to do that, the solenoidal system is stimulated by an AC source, with a $V_{rms} = 100mV$ and with a frequency varying from 20 Hz to 2 MHz. For the purpose of our analisys, it was more useful to represent the variation of the real part of the impedance (R - Resistance) and the complex part (X - Reactance) in relation with the values of the system in idle condition. In this way, it is more evident which is the contribution of the electromotive force generated by the induction mechanism.
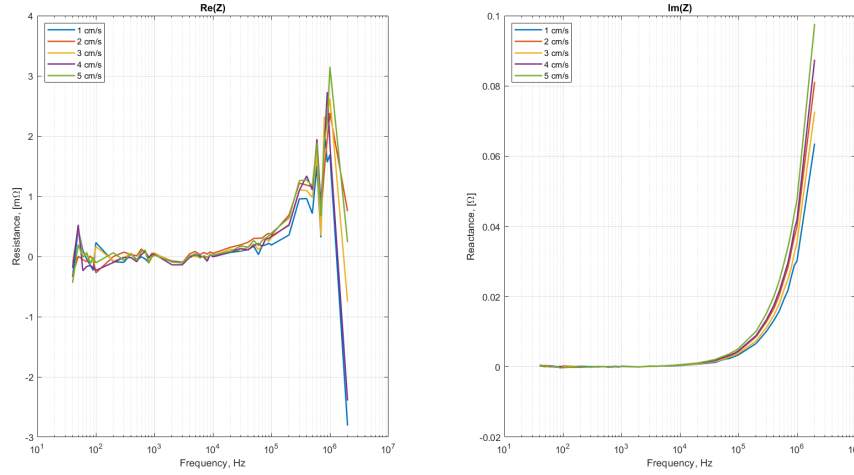

Figure 5.3. Relative impedance measurement of EFH3 solution at $\Phi = 0.02$ (dilution with kerosene). On the left, it is represented the real part of the impedance (R - Resistance) and on the right side there is the complex part of the impedance (X - Reactance).

Considering the model developed for the evaluation of the electromotive force generated by the system (Eq.2.76), it is possible to imagine that the system generates electromotive force from the variation of the magnetic susceptibility inside the solenoid, or rather, as a solenoid that changes its inductance according to the velocity of the inner fluid. In fact, observing the reactance plot, it is possible to see that the complex part of the system (the one associated to the inductive behaviour) changes according to the velocity of the fluid. This will be better clarified with the evaluation of the equivalent circuit model of the device.

For what concerns the voltage and current behaviour of the device, we notice that the two trends are quite related, because when the mean velocity of the fluid reaches 3 cm/s there is a decrease and subsequently an increase of both parameters. This is
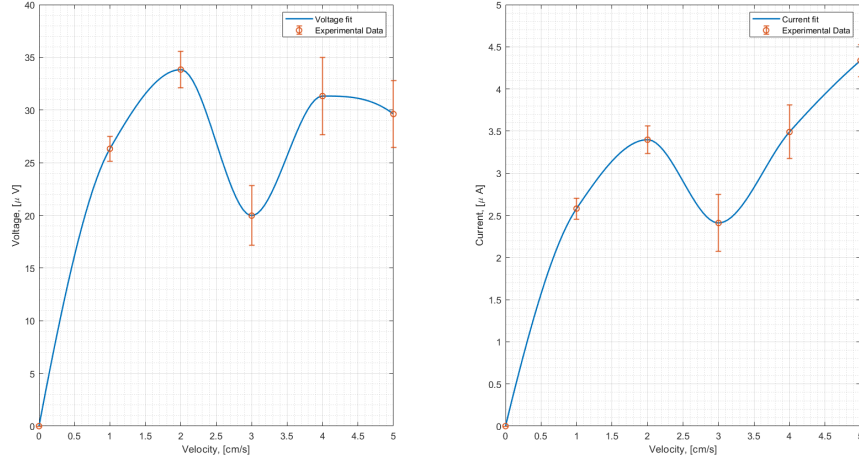
79

Figure 5.4. Voltage and Current characterization, as function of the mean velocity of the ferrofluid $\Phi = 0.02$. The error is calculated considering the standard deviation of the filtered subset of data, while the measure point represents the median of the data set, subtracting the idle condition contribution.

a direct evidence of the passive nature of the electrical characteristics of the device. Thus, it is possible to model the source as a electromotive force generator and the corresponding current associated to the resistive nature of the coil.

From a fluid dynamic point of view, we suppose that the negative variation of the voltage at 3 cm/s can be associated to a fluid transition from laminar flow to turbolent flow. This is mainly due to the fact that during the sizing of the device, we didn't take into account the magnetoviscous effects. This transition gives rise to "recirculation zones", where the velocity profile of the fluid is not anymore described by a Poiseuille flow, but there are different components of the velocity that point in the opposite direction of the fluid flow. Therefore, the evaluation of the mean velocity implies a reduction of the global electric characteristics of the system. This could be modeled reversing the cause with the effect, an so considering a "channel throttling", or better a sudden change of the geometry in the pipe system.

This is an evidence of the non linear dependence of the motion generation with respect to recovery part of the system. However, increasing again the mean velocity of the fluid, there is again a related increase of the voltage and current characteristics. Furthermore, it is possible to do an interesting relation between the voltage variation and the reactance component of the impedance: the increasing trend of the reactance follows the same behaviour of the voltage variation. This means that the time variation of the inductance is accountable to the electromotive force generation, as it was possible to suppose considering the time variation of the magnetic flux.
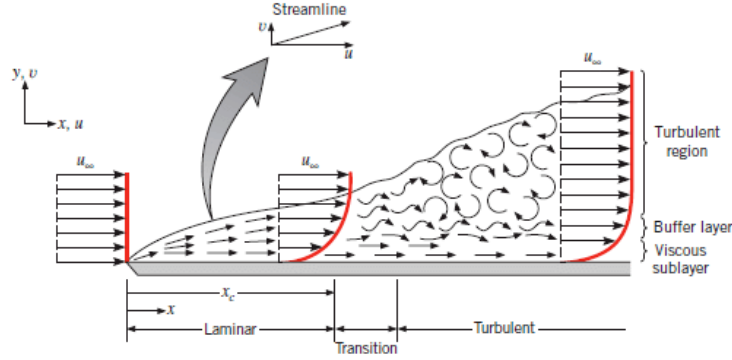
Figure 5.5.   Representation of the laminar to turbolent transition in the ferrofluid. On the bottom side of the fluid, the flow remains laminar since the magnetoviscous effects are more evident in presence of higher magnitude magnetic field.

For what concerns the electrical power analysis, the system reaches a voltage peak with a velocity of 2 cm/s, where the associated electromotive force has a value of 34 μV and the relative current has a value of 3.4 μA . Moreover, it is important to consider that the current generated in the device produces an induced magnetic field inside the coil that should perturb the motion of the magnetic fluid. In this case, it is evident that this perturbation is negligible, because the current behaviour follows linearly the same voltage behaviour. Finally, supposing that the output power generated by the device is the product of V_{OC} and I_{SC}, it reaches P = 0.115 nW in a volume of V = 7.85 mL. Therefore, the power per unit volume of ferrofluid at a concentration of 2% is equal to 14.64 μW/L (v = 2 cm/s). Note that in a real waste heat to power application, the evaluation of the output power should be done considering different resistive loads and consequently, evaluating the voltage and the current in each working condition.

5.1.2   Volume concentration 4%

In this case, the impedance behaviour of the system is completely different with respect to the previous one. In fact, the reactance component changes its concavity with respect to the previous case, where the ferrofluid concentration was 2%. This means that the internal dynamics is more influenced by the magnetoviscous effects, because we are increasing the magnetization component of the fluid. What is possible to suppose from this analysis is that we are introducing a non-linear component in the fluid motion, due to the complex distribution of magnetic field along the motion direction. Thus, this brings to a transition from laminar to turbulent flow that is evident at velocity of 1 cm/s. What is possible to suppose in this case is that the mean velocity in the extraction region of the pipe presents more distributed recirculation modes along the normal direction of the flow.
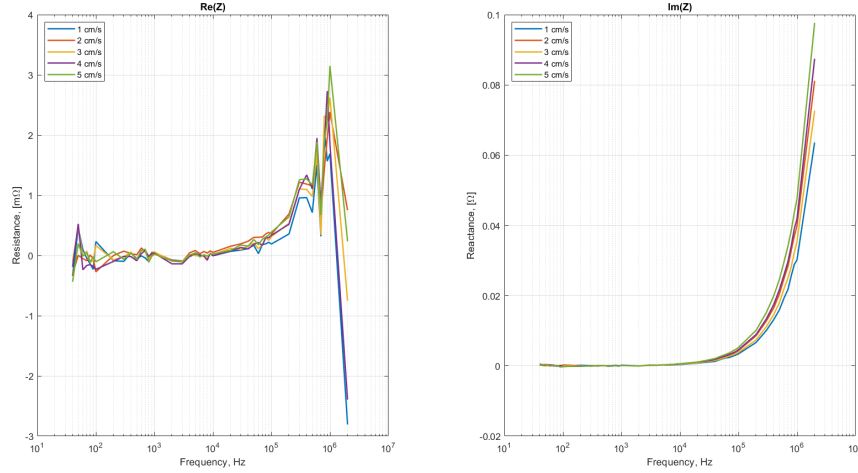

Figure 5.6.   Relative impedance measurement of EFH3 solution at $\Phi = 0.04$ (dilution with kerosene). On the left, it is represented the real part of the impedance (R - Resistance) and on the right side there is the complex part of the impedance (X - Reactance).

However, considering Eq.2.76, the voltage and current behaviour of the system can be easily explained in this way: if we consider that the fluid component which is in the bottom part of the pipe (near to the magnet source) becomes more viscous, the velocity along the motion direction decreases dramatically. The electromotive force is mostly related to the internal product between the magnetization field and the velocity field $(\nabla \mathbf{M}(\mathbf{r}) \cdot \mathbf{v}_p(\mathbf{r}))$. Therefore, there will be a reduction in the variation of the magnetic flux, or better there will exist a trade off between the motion generation part (velocity dependence) and the recovery part (magnitude

of the permanent magnets and concentration of the ferrofluid). So, it is possible to say that the two phenomena are mediated by the action of the magnetoviscous effect.
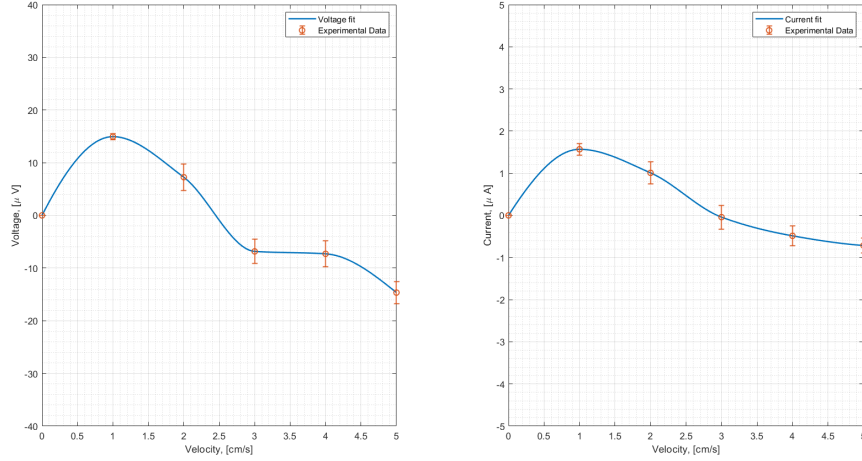

Figure 5.7.   Voltage and Current characterization, as function of the mean velocity of the ferrofluid $\Phi = 0.04$.

5.1.3   Volume concentration 6%

In this last case, where the concentration of the magnetite fraction is further increased, the laminar flow associated to the fluid dynamics is not anymore present even at v = 1 cm/s. This can be justified considering the reactance associated to the system: the inductive component of the fluid in the different operation conditions highlights a negative variation with respect to the idle case. Therefore, in the region where the magnetic field has an higher magnitude component (bottom of the pipe) the velocity profile is characterized by an opposite direction component with respect to the gradient of pressure induced by the peristaltic pump.

So, the voltage and current characterization can give us some information about the fluid motion in the pipe, but the results can not be used anymore for the output power characterization.

However, despite to the previous case, the voltage and current have a non comparable behaviour, meaning that the generation of current produces an induced magnetic field that perturbs the fluid motion. If we want to avoid this counter effect, it will be not possible to use the electromagnetic energy as a waste heat to power application, because this kind of recovery technique is more suitable for energy storage using batteries, supercapacitors, or in general devices that have an
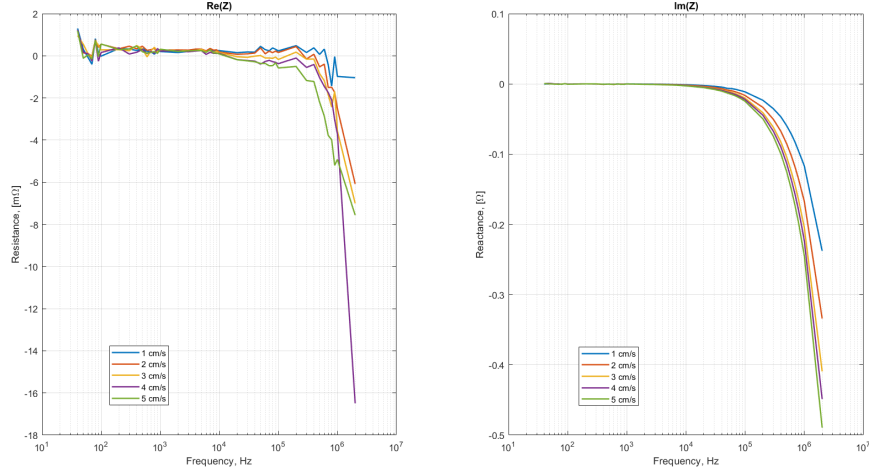
Figure 5.8.   Relative impedance measurement of EFH3 solution at $\Phi = 0.06$ (dilution with kerosene). On the left, there is represented the real part of the impedance (R - Resistance) and on the right side there is the complex part of the impedance (X - Reactance).

high intrinsic resistive and capacitive component. This also means that the electromotive force associated to the fluid motion can be increased simply introducing a larger density of coil in the extraction region.
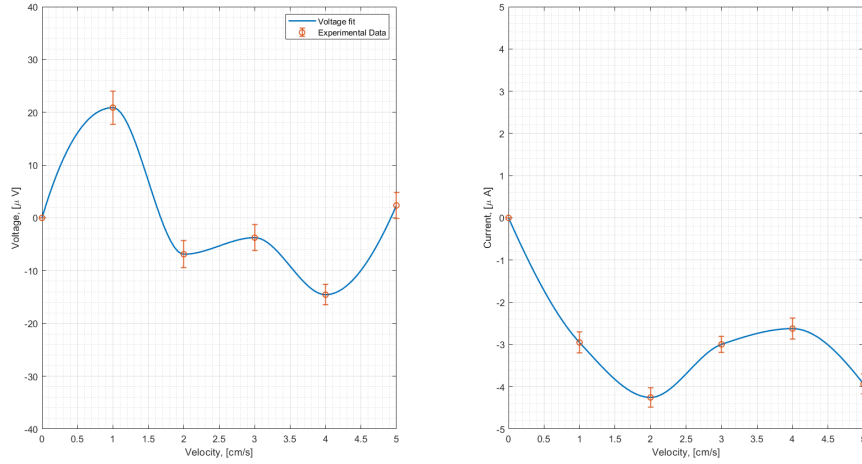

Figure 5.9.   Voltage and Current characterization, as function of the mean velocity of the ferrofluid $\Phi = 0.06$.

5.2   Capacitive characterization of Water-Titanium Dioxide solution

The procedure to collect data from the capacitive characterization of the triboelectric effect consists in the evaluation of the charge accumulation on the aluminum electrode, by means of open-circuit voltage and short-circuit current measurements. The main problem associated to this kind of analysis is the repeatability of the measurements. The key point in this case was to define a reference electrode, which has been identified as the common ground of the measurement instrumentation.

In order to verify the effective action of the triboelectric effect, we did a preliminary analysis on the time evolution of voltage and current, changing the operation condition of the pump. In particular, it is possible to observe that there is a direct relation between the variation of the velocity in the pipe and the generation of a voltage on the electrode. Moreover, when the pump is turned off, it is possible to observe a standard exponential decrease of the output voltage associated to a RC circuit.
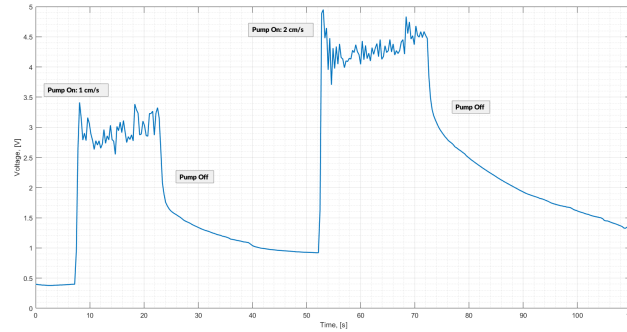

Figure 5.10.   Evidence of triboelectric effect from Voltage-Time behaviour of TiO_2 solution.

Another important consideration that it is necessary to do is the high noise level of current measurements with respect to the environmental conditions in the laboratory. In order to reduce the vibrational noise due to the peristalsis motion of the fluid in the pipe, we decided to proceed with a frequency analysis to observe the existence of modes besides the fundamental one (DC source).

In particular, a Fast Fourier Transform (FFT) is applied on the current measurements. We did not perform the same analysis on the voltage measurements, because the sensitivity of the system was not sufficiently high in order to study this noise phenomenon.
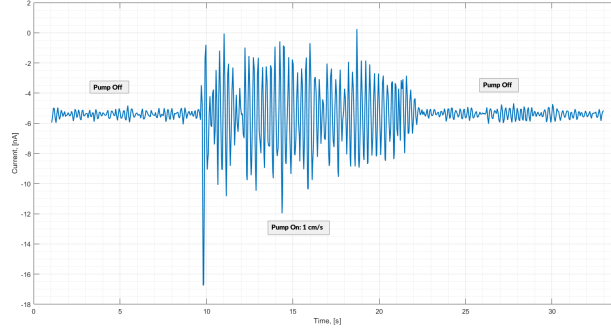
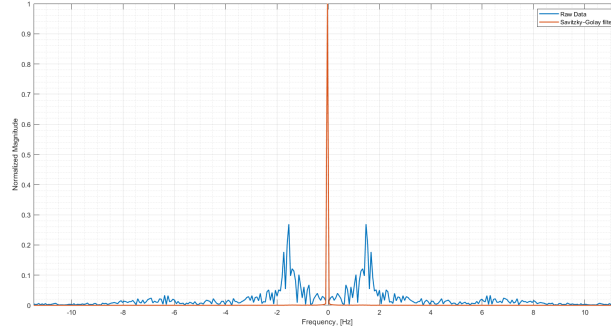Figure 5.11. Evidence of triboelectric effect from Current-Time behaviour of TiO_2 solution.

Figure 5.12. Example of frequency analysis on the current behaviour of pure water solution at v = 3 cm/s, before and after the filtering operation.

To better understand the direct link between the peristalsis motion and the frequency modes generation, we chose to perform a Gaussian fit on the Fourier Transform of the current measurements. This gave us important information about the frequency shift of the modes when the velocity of the flux is changed, the relative power of the mode with respect to the fundamental one and the Full Width at Half Maximum (FWHM) associated to each mode.

After this previous analysis, we selected a proper filtering window for the Savitzky-Golay filter to reduce the vibrational noise given by the pulsed motion of the fluid. A detailed analysis on the different operation condition is provided in the next sections. Finally, the procedure to evaluate the voltage and current generated by the triboelectric effect is the same as the inductive characterization: choose a subset of data neglecting the transient and filtering these data using a moving average filter.
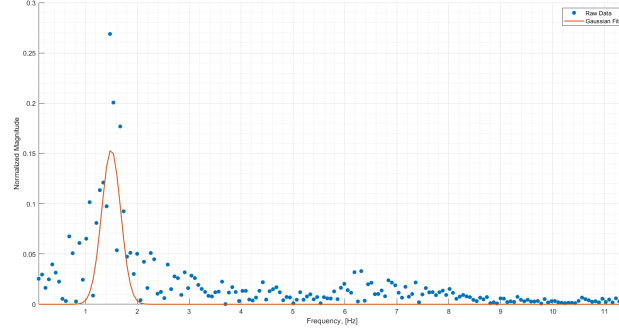
Figure 5.13.   Gaussian interpolation of the first mode associated to the current behaviour of pure water solution at v = 3 cm/s.

5.2.1   Pure Water

First of all, we tested the pipe system using pure water (purchased by Carlo Erba), characterized by an electrical resistivity of 12.8 MΩ/cm.

From the frequency analysis, it was possible to understand the dynamic behaviour of the first mode. In particular, in Tab.5.2.1 the values associated to the Gaussian interpolation of the first mode are reported.
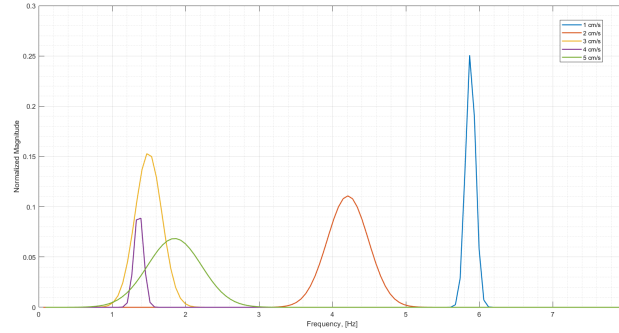

Figure 5.14.   Gaussian interpolation of the first mode associated to the fluid motion at different mean velocities in the case of pure water solution. It is modeled as a Gaussian White Noise centered in the Mode Frequency Peak.

The relative amplitude is measured with respect to the amplitude peak of the fundamental mode (DC source). So, the reported percentage represents the amount of averaged power that is brought by the peristaltic motion of the fluid inside the pipe, due to the time variation of the pressure generated by the pump. Moreover, the Mode Frequency Peak (MFP) can give us an information about the frequency shift of this mode: it is evident from the results that a trend exists in which the

frequency decrease when the mean velocity of the fluid grows up. This can be related to the machanical response in frequency of the pump-table system, where the pipe is anchored. Therefore, considering that the pump should be mechanically decoupled from the support surface (in our case a laboratory table), we observed that there will be always a vibrational component associated to rotational speed of the rotor of the pump. Hence, this noise must be not considered in the output power characterization and therefore it must be filtered by using a digital filter, that in our case has been identified as a first order Savitzky-Golay.

	Relative Amplitude	**Mode Frequency Peak (Hz)**	**FWHM (Hz)**
1 cm/s	25%	5.88	0.23
2 cm/s	11%	4.21	0.93
3 cm/s	15%	1.50	0.61
4 cm/s	9%	1.36	0.21
5 cm/s	6%	1.85	1.22

Table 5.1. Frequency analysis on the first mode associated to the current measurement of pure water sample.
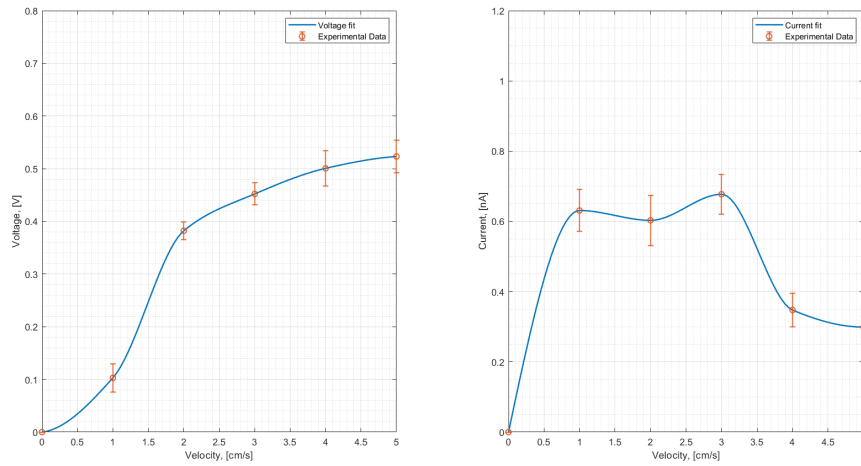

Figure 5.15. Voltage and Current characterization, as function of the mean velocity of pure water.

Once we set the filtering window in order to reduce this vibrational noise component, we proceded to measure the open-circuit voltage and the short-circuit current

associated to the system.

The voltage has an increasing behaviour with respect to the mean velocity and it reaches a peak at v = 5 cm/s, V_{OC} = 510 mV. However, the current has a different behaviour, since after that the velocity overcomes a value of v = 3 cm/s, it starts to decrease. In this case, the current peak is reached at v = 3 cm/s, with a value of I_{SC} = 680 pA.

As in the inductive case, it is possible to evaluate the output power by simply doing the product of V_{OC} and I_{SC}. The maximum value of the power is obtained at 3 cm/s, where P = 0.306 nW in a reference surface of S = 4.14 × 10^{-4} m^2, given by the geometrical properties of the aluminum electrode. So, with this setup, it is possible to reach a power per unit surface of P_S = 0.739 μW/m^2. As in the inductive case, a more detailed analysis about the output power characterization should be provided by evaluating the voltage and the current in presence of a load.

5.2.2 Titanium Dioxide - Volume concentration 1%

In this case, the preliminary analysis on the frequency behaviour shows that the mechanical properties of the fluid (variation of density and viscosity) give rise to a reduction of the noise power with respect to the velocity variation of the system. This implies that this first mode generation is associated to the fluid dynamic properties of the system and so, it is related to the peristaltic motion on the tube. As in the previous case, we proceeded to filter the data before doing computation of the output power of the system.
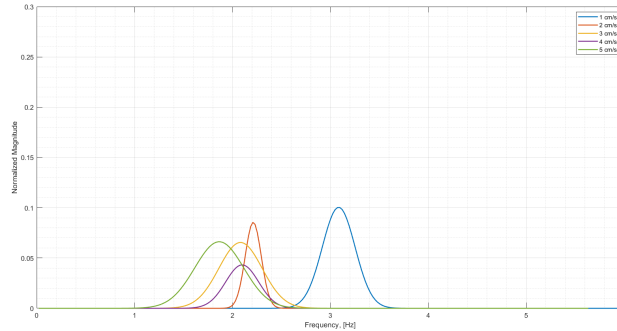

Figure 5.16. Gaussian interpolation of the first mode associated to the fluid motion at different mean velocity in the case of titanium dioxide solution.

For what concerns the evaluation of V_{OC} and I_{SC}, it is evident from Fig.5.2.2 that the electrical characterization has a behaviour completely different with respect to the case of pure water. First of all, it is possible to observe an increase of magnitude in voltage and current, at velocity lower than v = 2 cm/s. Nevertheless, increasing further the mean velocity of the fluid in the pipe, there is an inversion

	Relative Amplitude	Mode Frequency Peak (Hz)	FWHM (Hz)
1 cm/s	10%	3.08	0.33
2 cm/s	8%	2.21	0.26
3 cm/s	6%	2.08	0.74
4 cm/s	4%	2.09	0.56
5 cm/s	6%	1.86	0.83

Table 5.2. Frequency analysis on the first mode associated to the current measurement of titanium dioxide sample.

of the increasing trend in voltage measurements. This phenomenon can be related to the friction reduction between the solution and the pipe's wall, due to the fact that, overcoming a certain static accumulation of charges on the wall it is possible that the Coulomb repulsion acts actively on the fluid motion. This causes a change of operation conditions, passing from a slip condition to a no-slip condition, or rather when adhesion is stronger than cohesion. This could be justified doing a profilometry analysis on the wall of the pipe.

At v $= 3$ cm/s, the $V_{OC} = 560$ mV and the associated $I_{SC} = 850$ pA. This means that the output power reaches a value of P $= 0.476$ nW and so, there is an amelioration of 64% with respect to the case of pure water case. So, with this setup, it is possible to reach a power per unit surface of P$_S = 1.212$ μW/m^2.
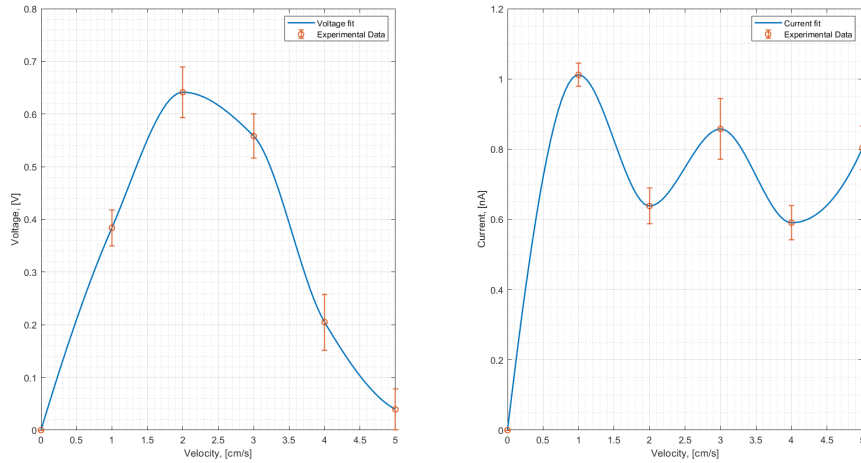

Figure 5.17. Voltage and Current characterization, as function of the mean velocity of the titanium dioxide solution, $\Phi = 0.01$.

Chapter 6

Conclusions and Future Perspectives

The last electrical characterization analysis that is possible to do with the collected data is the evaluation of an equivalent circuit. This is a very useful way of predicting or understanding the operation of the apparatus. In fact, the deconstruction of the physical behaviour of a complex mechanism, such as the generation of a electromotive force from a hydrodynamic machine, requires a set of simplifications. In particular, the best choice is to define a lumped-model, in which each element of the electric circuit is associated to a physical mechanism.
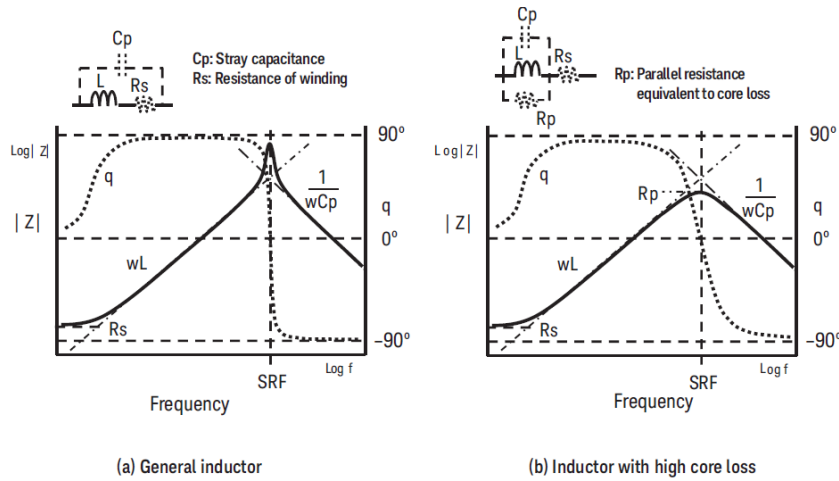

Figure 6.1. Bode diagram representation of the equivalent electrical model of an inductor system (L). Rs represents the internal resistance of the copper cable (winding), Cp is the stray capacitance of the system and Rp core losses, that can be represented as the cumulative effect of Brownian and Neél relaxation, related to the so called Eddy Current.

In the case of the ferrofluid system, the best representation is defined by the equivalent model of an inductor with high core loss, since the device under test was subjected to a mechanical perturbation of the magnetic permeability in the core region. To verify this assumption, it is possible to represent the reactance and the resistance in a Bode Diagram and in a Nyquist plot. From the Bode Diagram (Fig.**??**.3), it is clear that the impedance behaviour highlights a resistive component in series with an inductive component. However, the span of frequencies under test do not allow to confirm the modeling assumption, since it is not evident to observe a resistive component in parallel with the inductor that would have resulted in a kink or change of the slope. So, we can do the assumption that $Rp > 10^2 \ \Omega$.
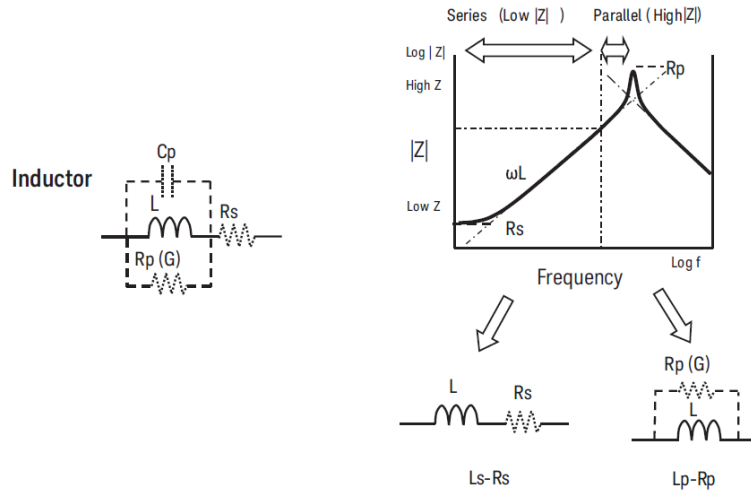
Figure 6.2. Different behaviour of the magnitude of an inductor system, evaluated at different frequencies. W

Thus, the Nyquist plot (Fig.6.4) can show us this particular behaviour. The resistance and the reactance present an increasing behaviour as the frequency increases. So, there must be a reistive component in parallel with the inductor part, that is physically associated to the core losses in the solenoid.

This model is a preliminary representation of the physical phenomena associated to the recovery mechanism of the system. However, from this simple analysis, it is possible to figure out the values associated with each component of the circuit, at different operation conditions.

From the equivalent circuit, it is possible to obtain the impedance characterization as a function of the circuit parameters.

$$Z = R + jX = Rs + \frac{Rp\,(\omega L)^2}{Rp^2 + (\omega L)^2} + j\frac{Rp^2\,\omega L}{Rp^2 + (\omega L)^2} \tag{6.1}$$
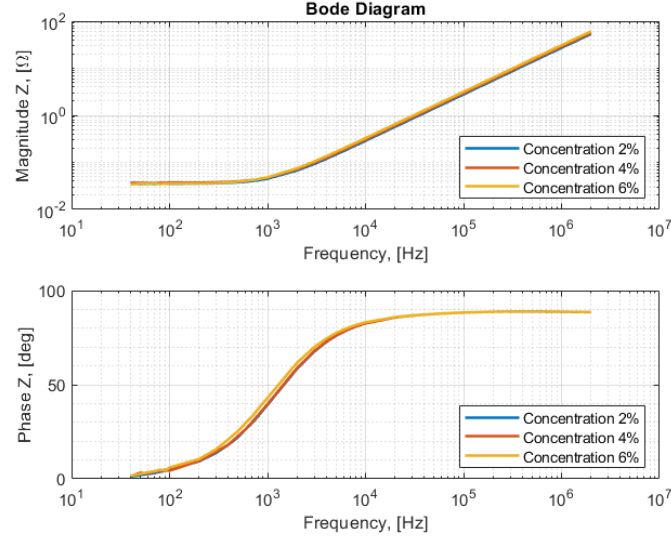
Figure 6.3. Bode diagram of the inductive system (idle condition) at different concentrations.
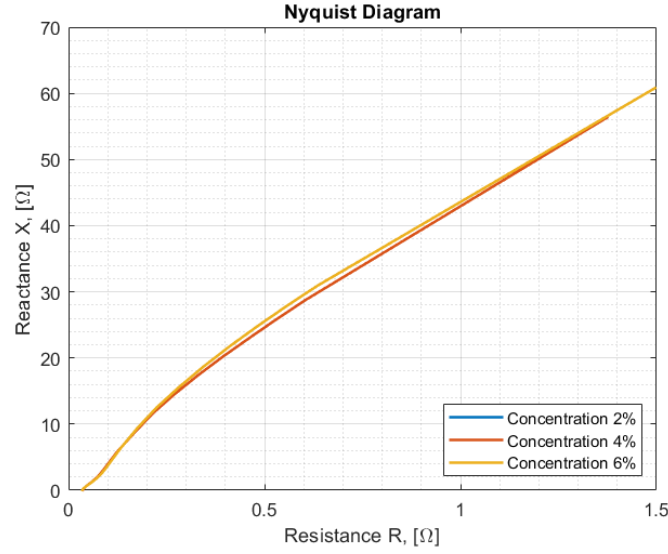

Figure 6.4. Nyquist diagram of the inductive system (idle condition) at different concentrations.

$$R = Rs + \frac{Rp\,(\omega L)^2}{Rp^2 + (\omega L)^2} \qquad\qquad X = \frac{Rp^2\,\omega L}{Rp^2 + (\omega L)^2} \qquad (6.2)$$

93

	Rs (mΩ)	Rp (Ω)	L (μH)
Offset	35.268	402.41	4.187
1 cm/s	34.928	403.83	4.192
2 cm/s	34.954	403.65	4.193
3 cm/s	35.159	403.62	4.193
4 cm/s	35.078	404.21	4.194
5 cm/s	34.830	404.09	4.195

Table 6.1.   Electrical parameters of the FF at 2% of concentration, evaluated from the equivalent circuit model.

	Rs (mΩ)	Rp (Ω)	L (μH)
Offset	36.946	399.13	4.405
1 cm/s	36.336	399.53	4.407
2 cm/s	36.598	399.79	4.404
3 cm/s	35.993	399.11	4.403
4 cm/s	36.081	399.27	4.403
5 cm/s	36.046	398.82	4.403

Table 6.2.   Electrical parameters of the FF at 4% of concentration, evaluated from the equivalent circuit model.

	Rs (mΩ)	Rp (Ω)	L (μH)
Offset	34.137	479.50	4.771
1 cm/s	35.433	475.74	4.751
2 cm/s	35.325	475.74	4.744
3 cm/s	35.097	474.74	4.738
4 cm/s	35.367	473.69	4.735
5 cm/s	35.323	473.89	4.732

Table 6.3.   Electrical parameters of the FF at 6% of concentration, evaluated from the equivalent circuit model.

The variation of the series resistance Rs can be associated to the generation of an electromotive force, while the change in magnitude of the parallel resistance Rp represents the variation of core losses in the solenoid, due to the fact that the motion in the fluid is characterized by recirculation regions of the fluid. However, it is interesting to note that also the inductance varies with the operation condition of the system. This could be associated to a more complex modelization of the fluid system.

Regarding the capacitive characterization, Ravelo et al.[33] provide a modelization of the triboelectric phenomenon in a liquid system, mainly based on the work of Touchard [30]. In particular, the system can be represented using a simplified Norton-Thevenin equivalent circuit, in this case an RC circuit.
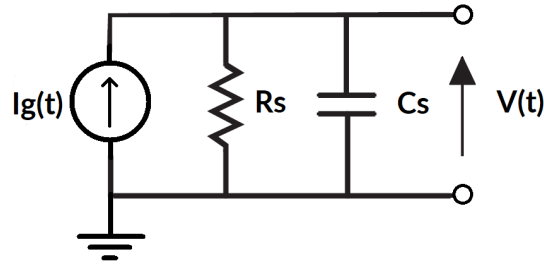

Figure 6.5.   Equivalent electrical model of the triboelectric system.

The capacitive and resistive component can be associated respectively to the dielectric and the conductive properties of the fluid system. Both of these parameters are also related to the geometrical parameters that define the extraction region.

$$Cs = \epsilon_0 \epsilon_r \, \frac{\Sigma}{d} \qquad\qquad Rs = \frac{1}{\sigma} \, \frac{t}{\Sigma} \qquad\qquad I_g = N \, e \, v \qquad (6.3)$$

where ϵ_r is the relative dielectric constant of the fluid, σ is the conductivity of the fluid, Σ is the internal surface of the electrode, d is the distance between the electrodes, t is the thickness of the electrode, N is the number of charges that can be extracted by means of the triboelectric effect, e is the charge of the electron and v is the velocity of the fluid on the wall of the pipe system.
The current generation represents the extraction of the electrons from the fluid solution to the wall of the pipe system, so it is directly linked to the carrier concentration and the velocity of the fluid. In this case, the match between the materials is important in order to define the charge density that can be obtained from the triboelectric effect. In particular, the exchange of carriers is related to the energy band diagram of the two materials and to the temperature of the system (Fermi-Dirac distribution).

All the considerations that we have done should be supported by a simulation of the physical phenomena, in order to have a better understanding of the global behaviour of the system.

However, this analysis shows that it is possible to extract energy from a liquid triboelectric system. In particular, dispersing titania powder in a pure water solution can bring an enhancement of the output power characteristic of 64% (from 0.739 μW/m^2 to 1.212 μW/m^2). For what concern the ferrofluid characterization, it was possible to introduce a first analysis on the electric characterization of magnetic fluid. In the future, it will be possible to investigate if this kind of characterization can give information about the motion in a fluid, enriched with magnetic nanoparticles. About the CERES project, a direct evidence of the possibility to extract energy from the fluid motion has been highlighted. In particular, at a mean velocity of 2 cm/s it was possible to generate 14.64 μW/L of output power per unit volume. This velocities are compatible with the magnitude of the speed generated by natural convection. Mixing triboelectric and magnetic effect in the CERES system will be an excellent solution in order to guarantee a stable extraction of electric power from low enthalpy waste heat sources: observing the voltage and current results from the two effects, it is clear that the triboelectric effect can generate higher voltages at lower current with respect to the magnetic induction. This means that if the two effects are correctly coupled, the time variation of the output power, given by the velocity oscillation in the toroidal reactor, can be easily converted in DC source as a linear power supply.

Finally, it was possible to evaluate a mechanical-electrical efficiency, considering the steady state operation of the fluid in the extraction volume. It is simply evaluated considering the electrical power extracted by the system (inductive of capacitive) divided by the difference of initial and final kinetic energy in the region of extraction. From an engineering estimation it is possible to assume that the variation of the velocity in the pipe will not overcome the 10% of the initial velocity. Thus, considering the ferrofluid concentration at 2% ($\rho = 866$ kg/m^3) and the power per unit volume evaluated for $v_i = 2$ cm/s we obtain that:

$$\eta_{Inductive} = \frac{2P_V}{0.19\rho \langle v_i \rangle^2} = 4.44\% \qquad (6.4)$$

where P_V is the power per unit volume, v_i is the initial and the final velocity in the pipe system and ρ is the density of the ferrofluid solution.

Using the same considerations for the triboelectric recovery, evaluated for $v_i = 3$ cm/s and $\rho = 1030$ kg/m^3, we obtain that:

$$\eta_{Capacitive} = \frac{2P_S}{0.19\, t\, \rho \langle v_i \rangle^2} = 12.51\% \qquad (6.5)$$

where P$_S$ is the power per unit surface and t is the thickness of the electrode.

6.1 Future Optimization

The experimental setup for the electrical characterization will probably introduce some relevant changes in the future, mainly based on the geometry and the installation of the magnets. In particular, from the results obtained it is possible to identify several lines of research:

- Improvement of the characterization system considering the magnetoviscous effect and leading to a change of the pumping mechanism (from peristalsis motion to constant pressure system).

- Synthesis and characterization of a multiphase colloidal system based on ferrofluid and TiO_2 powder, which give rise to a non-competitive combination of magnetic and triboelectric effect.

- Characterization of the TiO_2 colloidal system, through the evaluation of the zeta potential as a function of the pH of the solution. Understand the effect of the pH with respect to the charge accumulation given by the triboelectric effect.

- Validation of the characterization system though multiphysics simulation. Also, it is important to understand if the characterization method is able to give indications about the motion of a magnetic fluid in a pipe. This can be done coupling the system with a velocimetry analysis (doppler ultrasound velocimetry).

- Evaluation of the triboelectric effect in the CERES tank, considering the convection mechanisms that are established from the temperature variations.

- Use of FEP or PTFE as confining materials in the CERES system and installation of aluminum ring electrodes for the evaluation of the triboelectric effect in the WHR setup. It will be also important to analyse how the internal active surface of the wall can be functionalized with nanostructures.

- Considering Eq.2.76, in the CERES system will be more useful to install magnetic rings in order to extract electrical energy in a more efficient way and also to guarantee a toroidal motion of the magnetic particles in the tank.

- Since we have understood from the ferrofluid characterization that the system is more suitable for the accumulation of electrical energy, it will be more useful to increase the density of windings in the extraction region. Finally, the system should be converted in DC source and connected to an array of supercapacitors.

Bibliography

[1] International Energy Agency. "World Energy Outlook". In: (2018).

[2] Gregorc Boštjan and Saša Erlih. "Waste Heat Utilization of Hydro-Power Plants". In: *Conference on exploitation of waste heat potentials in Europe.* 2017 and references therein.

[3] *Waste Heat Recovery: Technology and Opportunities in the U.S. Industry.* 2008.

[4] Amelia Elson, Rick Tidball, and Anne Hampson. *Waste Heat to Power Market Assessment.* 2015.

[5] Oriol Gavaldà et al. *Report of different options for renewable energy supply in Data Centres in Europe.* 2014.

[6] Alessandro Chiolerio and Marco B. Quadrelli. "Colloidal Energetic Systems". In: *Energy Technology* 7.5 (2019). DOI: 10.1002/ente.201800580.

[7] H.B. Callen. *Thermodynamics and an Introduction to Thermostatistics - Second Edition.* Wiley, 1985, pp. 5–199. ISBN: 978-0-471-86256-7.

[8] Thorade M. and Saadat A. "Partial derivatives of thermodynamic state properties for dynamic simulation". In: 70 (2013), pp. 3479–3503. DOI: 10.1007/s12665-013-2394-z.

[9] Bridgman P. W. "A complete collection of thermodynamic formulas". In: 3 (1914), pp. 273–281. DOI: 10.1103/PhysRev.3.273.

[10] Lungu R. P. "Thermodynamics of electric and magnetic systems". In: *Trends in Electromagnetism - From Fundamentals to Applications* (2012), pp. 113–152. DOI: 10.5772/38947.

[11] Karl A. Gschneidner Jr Vitalij K. Pecharsky. "Magnetocaloric effect and magnetic refrigeration". In: *Journal of Magnetism and Magnetic Materials* (1999). DOI: 10.1016/S0304-8853(99)00397-2.

[12] Binns Chris. *Nanomagnetism: Fundamentals and Applications.* Elsevier, 2014, pp. 1–15. ISBN: 978-0-08-098353-0.

[13] Sergei Gubin et al. "Magnetic nanoparticles: Preparation, structure and properties". In: *Russian Chemical Reviews* 74 (June 2005), pp. 539–574. DOI: 10.1070/RC2005v074n06ABEH000897.

[14] Stefan Odenbach. *Magnetoviscous Effects in Ferrolfuids*. New York: Springer, 2002, ISBN: 3-540-43068-7.

[15] Charles Kittel. *Introduction to Solid State Physics - 8th Edition*. Wiley, pp. 302–304. ISBN: 0-471-41526-X.

[16] Stephen D. Senturia. *Microsystem Design*. Kluwer Academic Publishers, 2002, pp. 319, 322–323. ISBN: 0-306-47601-0.

[17] R. E. Rosensweig. *Ferrohydrodynamics*. Mineaola, New York: Dover Pubblication, 2012, p. 25. ISBN: 978-0-486-78300-0.

[18] Timothy H Boyer. "The force on a magnetic dipole". In: *American Journal of Physics* (1988). DOI: 10.1119/1.15501.

[19] Raphaël Zanella. "Thermomagnetic Convection in Ferrofluids : Finite Element Approximation and Application to Transformer Cooling". In: (2019).

[20] Costica Caizer. *Nanoparticle Size Effect on Some Magnetic Properties*. June. 2015. ISBN: 9783319153384. DOI: 10.1007/978-3-319-15338-4.

[21] Stefan Odenbach and Mario Liu. "Invalidation of the Kelvin Force in Ferrofluids". In: *Physical Review Letters* (2000). DOI: 10.1103/PhysRevLett.86.328.

[22] Stefan Odenbach. *Ferrofluids: Magnetically Controllable Fluids and Their Applications*. New York: Springer, 2002, pp. 88–89. ISBN: 978-3-540-45646-9.

[23] Bruce A. Finlayson. "Convective instability of ferromagnetic fluids". In: *Journal of Fluid Mechanics* (1970), pp. 753–767. DOI: 10.1017/S0022112070000423.

[24] Sergey A. Suslov. "Themomagnetic convection in a vertical layer of ferromagnetic fluid". In: *Physics of Fluid* (2008), p. 20. DOI: 10.1063/1.2952596.

[25] Sergey A. Suslov et al. "Thermomagnetic convective flows in a vertical layer of ferrocolloid: Perturbation energy analysis and experimental study". In: *Physical Review E* 86 (2012), pp. 1–15. DOI: 10.1103/PhysRevE.86.016301.

[26] Elmo Benedetto. "Some remarks about flux time derivative". In: 28 (2017), pp. 23–27. DOI: 10.1007/s13370-016-0424-1.

[27] Zhong Lin Wang et al. *Triboelectric Nanogenerators*. Springer, 2016, pp. 3–105. ISBN: 978-3-319-40038-9.

[28] Zong-Hong Lin et al. "Water–Solid Surface Contact Electrification and its Use for Harvesting Liquid-Wave Energy". In: *Angewandte Chemie* (2013). DOI: 10.1002/ange.201307249.

[29] Hong-Yeol Park et al. "Water-Through Triboelectric Nanogenerator Based on Ti-mesh for Harvesting Liquid Flow". In: *Journal of the Korean Physical Society* (2018). DOI: 10.3938/jkps.72.499.

[30] Gérard Touchard. "Flow electrification of liquids". In: *Journal of Electrostatics* (2001). DOI: `10.1016/S0304-3886(01)00081-X`.

[31] M. EL-Adawy et al. "Numerical simulation of the electrical double layer development: physicochemical model at the solid and dielectric liquid interface for laminar flow electrification phenomenon". In: *IEEE Transactions on Dielectrics and Electrical Insulation* 18.5 (2011), pp. 1463–1475. DOI: `10.1109/TDEI.2011.6032817`.

[32] Thiago A. L. Burgo et al. "Where is water in the triboelectric series?" In: *Journal of Electrostatics* (2016). DOI: `10.1016/j.elstat.2016.01.002`.

[33] Ravelo et al. "Demonstration of the triboelectricity effect by the flow of liquid water in the insulating pipe". In: *Journal of Electrostatics* 69 (2011), pp. 473–478. DOI: `10.1016/j.elstat.2011.06.004`.

[34] Quadrelli M. Chiolerio A. "Smart Fluid Systems: The Advent of Autonomous Liquid Robotics". In: *Advanced Science* 4 (2017). DOI: `10.1002/advs.201700036`.

[35] J. Sindel J.H. Adair E. Suvaci. *Encyclopedia of Materials: Science and Technology.* Elsevier, 2001. Chap. Surface and Colloid Chemestry, pp. 1–10. ISBN: 978-0-08-043152-9.

[36] H. C. Hamaker. "The London – Van der Waals attraction between spherical particles". In: *Physica 4(10)* (1937), pp. 1058–1072. DOI: `10.1016/S0031-8914(37)80203-7`.

[37] E.M. Lifshitz. "The Theory of Molecular Attractive Forces between Solids". In: *Journal of Experimental Theoretical Physics* (1955), pp. 94–110.

[38] Noel Clark. "Ferromagnetic ferrofluids". In: *Nature* (2013). DOI: `10.1038/504229a`.

[39] Stefan Odenbach et al. *Colloidal Magnetic Fluids: Basics, Development and Application of Ferrofluids.* Springer, 2009, pp. 1–69. ISBN: 978-3-540-85386-2.

[40] Susan Mousavi, Sunil Kumar, and Sachin Khapli. "Properties of ferrolfuids". In: *Proceedings of the 22nd National and 11th International ISHMT-ASME Heat and Mass Transfer Conference* (2013). DOI: `10.13140/RG.2.1.3038.8320`.

[41] A O Ivanov, O B Kuznetsova, and I M Subbotin. "Magnetic properties of ferrofluid emulsions: the effect of droplets elongation". In: *Magnetohydrodynamcs* 49 (2013), pp. 287–292.

[42] A O Ivanov, O B Kuznetsova, and I M Subbotin. "Magnetic properties of ferrofluid emulsions: model of non-interacting droplets". In: *Magnetohydrodynamcs* 47 (2011), pp. 129–134.

[43] Yuri Dikansky, Anna Ispiryan, and Stanislav Kunikin. "On the temperature dependence of ferrofluid susceptibility". In: *EPJ Web of Conferences* 185 (2018), pp. 1–4. DOI: `10.1051/epjconf/201818509011`.

[44] J. Popplewell et al. "Thermal conductivity measurements on ferrofluids". In: *Colloid and Polymer Science* 260 (1982). DOI: `10.1007/BF01447973`.